This paper covers the content of papers 7B.1 & 7B.2 (File size for the 2 papers is 3,067 KB)

Short-Term Forecasting of Severe Convective Storms Using Quantitative Multi-Spectral, Satellite Imagery: Results of the Early Alert Project

William L. Woodley[1], Daniel Rosenfeld[2], Guy Kelman[2] and Joseph H. Golden[3]

[1]Woodley Weather Consultants, [2]Hebrew University of Jerusalem, [3]Cooperative Institute for Research in the Environmental Sciences

1.0 BACKGROUND

A team of research scientists has been working under the auspices of Woodley Weather Consultants (WWC) with the support of NOAA's Small Business Innovative Research Program (SBIR) to develop and test a method to provide satellite, microphysically-based, "Early Alerts" (EA) of severe convective storms (tornadoes, hail and strong, straight-line, downburst winds). The method objective is to predict when and where a severe weather is most likely to occur one to two hours prior to the actual event, potentially saving lives and property. This report documents the development and testing of the methodology, including its scientific basis and the underlying conceptual model, the initial work with AVHRR multi-spectral data from polar-orbiting satellites, the adaptation of the method to accept real-time GOES multi-spectral data, and the real-time testing of the method at the Storm Prediction Center in Norman, Oklahoma.

As discussed in Section 2.0 herein, the new method is based on a conceptual model that facilitates the inference of the vigor of severe convective storms, producing tornadoes and large hail, by using satellite-retrieved vertical profiles of cloud top temperature (T) and particle effective radius (r_e). The driving force of these severe weather phenomena is the high updraft speed, which can sustain the growth of large hailstones and provide the upward motion that is necessary to evacuate the violently converging air of a tornado. Stronger updrafts are revealed by the delayed growth of r_e to greater heights and lower T, because there is less time for the cloud and rain drops to grow by coalescence. The strong updrafts also delay the development of a mixed phase cloud and its eventual glaciation to colder temperatures. In addition to the presentation of the conceptual model and the derivation of the method, this section documents the initial testing of the concepts using multi-spectral AVHRR data from polar-orbiting satellites.

Even though this work validated the conceptual model, it had minimal practical forecast value because it was based on imagery that was available only once or twice per day. Greater image frequency was needed. Section 3 gives the results of initial testing under SBIR-1 of the concepts and method using GOES multi-spectral imagery that was available at 30 min intervals. The concepts and methods proved robust to this testing, and the question arose whether a

---

Corresponding author address: William L. Woodley, Woodley Weather Consultants, 11 White Fir Court, Littleton, Colorado 80127; e-mail:williamlwoodley@cs.com

real-time version of the method could be developed to improve severe storm watches and warnings. Doing this was the focus of SBIR-2. As discussed in Section 5.0, this entailed the development of a real-time version of the method that was tested at the Storm Prediction Center (SPC) during the spring of 2008.

2.0 INITIAL CONCEPTUAL TESTING

2.1 Scientific Basis

This study builds on the paper by Rosenfeld et al. (2007) that provides the scientific basis and background for the new conceptual model to be discussed here that facilitates the detection of the vigor of convective storms by remote sensing from satellites, based on the retrieved vertical profiles of cloud-particle effective radius and thermodynamic phase. Severe convective storms are defined by the US National Weather Service as having wind gusts > 58 mph, hail > 3/4 inch in diameter, or producing tornadoes. A major driving force of all these severe weather phenomena is the high updraft speeds, which can sustain the growth of large hailstones, provide the upward motion that is necessary for evacuating vertically the violently converging air of a tornado, or complemented strong downward motion, which results in downbursts and intense gust fronts. Wind shear provides additional energy for sustaining the dynamics of tornadic super-cell storms and squall lines that can re-circulate large hailstones and produce damaging winds. The respective roles of convective potential available energy (CAPE) and the 0-6 km vertical wind shear have been the main predictors for severe convective storms (Rasmussen and Blanchard, 1998; Hamill and Church, 2000; Brooks et al., 2003). The existence of wind shear and low-level storm relative helicity (rotation of the wind vector) were found to be associated with strong (at least F2) tornadoes (Dupilka and Reuter, 2006a and 2006b). However, even with small helicity, a steep low level lapse rate and large CAPE can induce strong tornadoes due to the large acceleration of the updrafts already at low levels (Davis, 2006). This underlines the importance of the updraft velocities in generating the severe convective storms, and the challenges involved in their forecasting based on sounding data alone.

The conceptual model of a satellite-observed severe storm microphysical signature that is addressed in this paper is based on the satellite-retrieved microphysical signature of the updraft velocity of the developing convective elements that have the potential to become severe convective storms, or already constitute the feeders of such storms. The severe storm microphysical signature, as manifested by the vertical profile of cloud-particle effective radius, is caused by the greater updrafts delaying to greater heights the conversion of cloud drops to hydrometeors and the glaciation of the cloud. The greater wind shear tilts the convective towers of the pre-storm and feeder clouds and often deflects the strongly diverging cloud tops from obscuring the feeders. This allows the satellite a better view of the microphysical response of the clouds to the strong updrafts. This satellite severe storm signature appears to primarily reflect the updraft speed of the growing clouds, which is normally associated with the CAPE. But wind shear is as important as CAPE for the occurrence of severe convective storms, in addition to helicity that is an important ingredient in intense tornadoes. It is suggested that the effectiveness of the satellite retrieved severe storm signature and inferred updraft speed may not only depend on the magnitude of

the CAPE, but also on the wind shear, and perhaps also on the helicity. This can occur when some of the horizontal momentum is converted to vertical momentum in a highly sheared environment when strong inflows are diverted upward, as often happens in such storms. While this study focuses on exploring a new concept of satellite application, eventually a combined satellite with a sounding algorithm is expected to provide the best skill.

2.1.1 Direct observations of cloud top dynamics for inferences of updraft velocities and storm severity

Updraft speeds are the most direct measure of the vigor of a convective storm. The updraft speeds of growing convective clouds can be seen in the rise rate of the cloud tops, or measured from satellites as the cooling rate of the tops of these clouds. A typical peak value of updrafts of severe storms exceeds 30 ms^{-1} (e.g., Davies-Jones, 1974). Such strong updrafts are too fast to be detected by a sequence of geostationary satellite images, because even during a 5 minute rapid scan an air parcel moving at 30 ms^{-1} covers 9 km if continued throughout that time (super-rapid scans of up to one per 30 – 60 s can be done, but only for a small area and not on a routine operational basis). But such strong updrafts occur mainly at the supercooled levels, where the added height of 9 km will bring the cloud top to the tropopause in less than 5 minutes. In addition, the cloud segments in which such strong updrafts occur are typically smaller than the resolution of thermal channels of present day geostationary satellites (5 to 8 km at mid latitudes). This demonstrates that both the spatial and temporal resolutions of the current geostationary satellites are too coarse to provide direct measurements of the updraft velocities in severe convective clouds. The overshooting depth of cloud tops above the tropopause can serve as a good measure of the vigor of the storms, but unfortunately the brightness temperatures of overshooting cloud tops do not reflect their heights due to the generally isothermal nature of the penetrated lower stratosphere.

Overshooting severe convective storms often develop a V shape feature downwind of their tallest point, which appears as a diverging plume above the anvil top (Heymsfield et al., 1983; McAnn, 1983). The plume typically is highly reflective at 3.7 μm, which means that it is composed of very small ice particles (Levizzani and Setvák, 1996, Setvák et al., 2003). A warm spot at the peak of the V is also a common feature, which is likely caused by the descending stratospheric air downwind of the overshooting cloud top. Therefore, the V-shape feature is a dynamic manifestation of overshooting tops into the lower stratosphere when strong storm-relative winds occur there. The observation of a V-shape feature reveals the existence of the combination of intense updrafts and wind shear. Adler et al. (1983) showed that most of the storms that they examined in the US Midwest (75%) with the V-shape had severe weather, but many severe storms (45%) did not have this feature. Adler et al. (1983) showed also that the rate of expansion of storm anvils was statistically related positively to the occurrences of hail and tornadoes. All this suggests that satellite inferred updraft velocities and wind shear are good indicators for severe storms. While wind shear is generally easily inferred from synoptic weather analyses and predictions, the challenge is the inference of the updraft intensities from the satellite data. The manifestation of updraft velocities in the cloud microstructure and thermodynamic phase, which can be detected by satellites, is the subject of the next section.

2.1.2 Anvil tops with small particles at -40°C reflecting homogeneously-glaciating clouds

Small ice particles in anvils or cirrus clouds typically form as a result of either vapor deposition on ice nuclei, or by homogeneous ice nucleation of cloud drops which occurs at temperatures colder than -38°C. In deep convective clouds heterogeneous ice nucleation typically glaciates the cloud water before reaching the -38°C threshold. Clouds that glaciate mostly by heterogeneous nucleation (e.g. by ice multiplication, ice-water collisions, ice nuclei and vapor deposition) are defined here as glaciating heterogeneously. Clouds in which most of their water freezes by homogeneous nucleation are defined here as undergoing homogeneous glaciation. Only a small fraction of the cloud drops freezes by interaction with ice nuclei, because the concentrations of ice nuclei are almost always smaller by more than four orders of magnitude than the drop concentrations (ice nuclei of ~0.01 cm^{-3} whereas drop concentrations are typically > 100 cm^{-3}) before depletion by evaporation, precipitation or glaciation. Therefore, most drops in a heterogeneously glaciating cloud accrete on pre-existing ice particles, or evaporate for later deposition on the existing cloud ice particles. This mechanism produces a glaciated cloud with ice particles that are much fewer and larger than the drops that produced them. In fact, heterogeneous glaciation of convective clouds is a major precipitation-forming mechanism.

Heterogeneously glaciating clouds with intense updrafts (>15 ms^{-1}) may produce large supersaturations that, in the case of a renewed supply of CCN from the ambient air aloft, can nucleate new cloud drops not far below the -38°C isotherm, which then freeze homogeneously at that level (Fridlind et al., 2004; Heymsfield et al., 2005). In such cases the cloud liquid water content (LWC) is very small, not exceeding about 0.2 g m^{-3}. This mechanism of homogeneous ice nucleation occurs, of course, also at temperatures below -38°C, and is a major process responsible for the formation of small ice particles in high-level strong updrafts of deep convective clouds, which are typical of the tropics (Jensen and Ackerman, 2006).

Only when much of the condensed cloud water reaches the -38°C isotherm before being consumed by other processes can the cloud be defined as undergoing homogeneous glaciation. The first in situ aircraft observations of such clouds were made recently, where cloud filaments with LWC reaching half (Rosenfeld and Woodley, 2000) to full (Rosenfeld et al., 2006b) adiabatic values were measured in west Texas and in the lee of the Andes in Argentina, respectively. This required updraft velocities exceeding 40 ms^{-1} in the case of the clouds in Argentina, which produced large hail. The aircraft measurements of the cloud particle size in these two studies revealed similar cloud particle sizes just below and above the level where homogeneous glaciation occurred. This means that the homogeneously glaciating filaments in these clouds were feeding the anvils with frozen cloud drops, which are distinctly smaller than the ice particles that rise into the anvils within a heterogeneously glaciating cloud.

In summary, there are three types of anvil compositions, caused by three glaciation mechanisms of the convective elements: (1) Large ice particles formed by heterogeneous glaciation; (2) homogeneous glaciation of LWC that was generated at low levels in the cloud, and, (3) homogeneous glaciation of newly nucleated cloud drops near or above the -38°C isotherm level. This

third mechanism occurs mostly in cirrocumulus or in high wave clouds, as shown in Figure 7a in Rosenfeld and Woodley (2003). The manifestations of the first two mechanisms in the composition of anvils are evident in the satellite analysis of cloud top temperature (T) versus cloud top particle effective radius (r_e) shown in Figure 1. In this red-green-blue composite brighter visible reflectance is redder, smaller cloud top particles look greener, and warmer thermal brightness temperature is bluer. This analysis methodology (Rosenfeld and Lensky, 1998) is reviewed in Section 2.2 of this paper. The large ice particles formed by heterogeneous glaciation appear red in Figure 1 and occur at cloud tops warmer than the homogeneous glaciation temperature of -38°C. The yellow cloud tops in Figure 1 are colder than -38°C and are composed of small ice particles that probably formed by homogeneous glaciation. The homogeneously glaciated cloud water appeared to have ascended with the strongest updrafts in these clouds and hence formed the tops of the coldest clouds.

The homogeneous freezing of LWC generated at low levels in convective clouds is of particular interest here, because it is indicative of updrafts that are sufficiently strong such that heterogeneous ice nucleation would not have time to deplete much of the cloud water before reaching the homogeneous glaciation level. As such, the satellite signature in the form of enhanced 3.7-µm reflectance can be used as an indicator of the occurrence of strong updrafts, which in turn are conducive to the occurrence of severe convective storms. This realization motivated Lindsey et al. (2006) to look for anvils with high Geostationary Operational Environmental Satellite (GOES) 3.9-µm reflectance as indicators of intense updrafts. They showed that cloud tops with 3.9-µm reflectance > 5% occurred for τ<100 s, where τ is the parameterized cloud drop residence time in the updraft between cloud base and the -38°C isotherm level. Lindsey et al. (2006) calculated τ according to eq. 1:

$$\tau = D_{LCL/-38} / w_{max} \quad (1)$$

where

$$w_{max} = (2\ CAPE)^{0.5} \quad (2)$$

and $D_{LCL/-38}$ is the distance [m] between the LCL and the -38°C isotherm level. The requirement for τ< 100 s for homogeneous glaciation can be contrasted with the in situ aircraft observations of glaciation time of about 7 minutes at temperatures of -32°C to -35°C (Rosenfeld and Woodley, 2000). This reflects the fact that actual updraft velocities are much smaller than w_{max}.

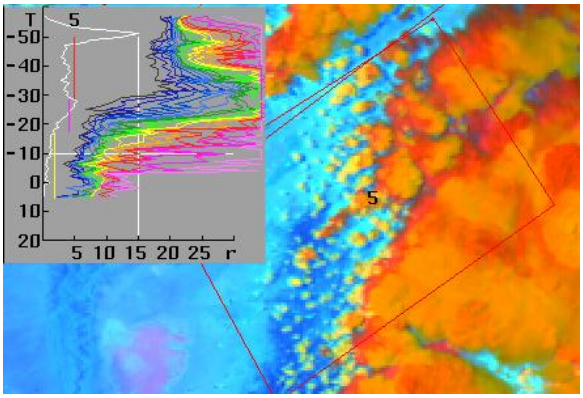

Figure 1: A T-r_e analysis of the cloud top microstructure of a Cb (cumulonimbus) that has an anvil partially formed by homogeneous freezing, where r_e is the cloud particle effective radius in µm. The image is based on a NOAA-AVHRR overpass on 8 June 1998, 22:12 UTC over New Mexico. The domain is 220x150 AVHRR 1-km pixels. The image is an RGB composite where the visible channel modulates the red, 3.7 µm reflectance modulates the green, and 10.8 µm brightness temperature modulates the blue (after Rosenfeld and Lensky, 1998). Brighter 3.7 µm reflectance (greener) means smaller cloud top particles. The inset shows

the T-r_e lines for the clouds in the marked rectangle. The different colored lines represent different T-r_e percentiles every 5% from 5% (left most line) to 100% (right most line), where the bright green is the median. The white line on the left side of the inset is the relative frequency of the cloudy pixels. The vertical lines show the vertical extent of the microphysical zones: yellow for the diffusional growth; green for the coalescence zone (does not occur in this case); pink for the mixed phase and red for the glaciated zone. The glaciated cloud elements that do not exceed the -38°C isotherm appear red and have very large r_e that is typical of ice particles that form by heterogeneous freezing in a mixed phase cloud, whereas the colder parts of the anvil are colored orange and are composed of small particles, which must have formed by homogeneous freezing of the cloud drops in the relatively intense updraft that was necessary to form the anvil portions above the -38°C isotherm.

The concept of "residence time" fails for clouds that have warm bases, because even with CAPE that is conducive to severe storms heterogeneous freezing is reached most of the time. This is manifested by the fact that clouds with residence times less than 100 s and hence with 3.9-μm reflectivities greater than 5%, were almost exclusively west of about 100°W, where cloud base heights become much cooler and higher (Lindsey, personal communications pertaining to Figure 7 of his 2006 paper).

Aerosols play a major role in the determination of the vertical profiles of cloud microstructure and glaciation. Khain et al. (2001) simulated with an explicit microphysical processes model the detailed microstructure of a cloud that Rosenfeld and Woodley (2000) documented, including the homogeneous glaciation of the cloud drops that had nucleated near cloud base at a temperature of about 9°C. When changing in the simulation from high to low concentrations of CCN, the cloud drop number concentration was reduced from 1000 to 250 cm^{-3}. Coalescence quickly increased the cloud drop size with height and produced hydrometeors that froze readily and scavenged almost all the cloud water at -23°C, well below the homogeneous glaciation level. This is consistent with the findings of Stith et al. (2004), who examined the microphysical structure of pristine tropical convective clouds in the Amazon and at Kwajalein, Marshall Islands. They found that the updrafts glaciated rapidly, most water being removed between -5 and -17°C, and suggested that a substantial portion of the cloud droplets were frozen at relatively warm temperatures.

In summary, the occurrence of anvils composed of homogeneously glaciated cloud drops is not a unique indicator of intense updrafts, because it depends equally strongly on the depth between cloud base and the -38°C isotherm level. The microphysical evolution of cloud drops and hydrometeors as a function of height above cloud base reflects much better the combined roles of aerosols and updrafts, with some potential of separating their effects. If so, retrieved vertical microphysical profiles can provide information about the updraft intensities. This will be used in the next section as the basis for the conceptual model of severe storm microphysical signatures.

2.2. A Conceptual Model of Severe Storm Microphysical Signatures

2.2.1 The vertical evolution of cloud microstructure as an indicator of updraft velocities and CCN concentrations

The vertical evolution of satellite-retrieved, cloud-top-particle, effective radius is used here as an indicator of the vigor of the cloud. In that respect it is important to note that convective cloud top drop sizes do not depend on the vertical growth rate of the cloud (except for cloud base updraft), as long as vapor diffusion and condensation is the dominant cause for droplet growth. This is so because: i) the amount of condensed cloud water in the rising parcel depends only on the height above cloud base, regardless of the rate of ascent of the parcel, and ii) most cloud drops were formed near cloud base and their concentrations with height do not depend on the strength of the updraft as long as drop coalescence is negligible.

The time for onset of significant coalescence and warm rain depends on the cloud drop size. That time is shorter for larger initial drop sizes (Beard and Ochs, 1993). This time dependency means also that a greater updraft would lead to the onset of precipitation at a greater height in the cloud. This is manifested as a higher first precipitation radar echo height. At supercooled temperatures the small rain drops freeze rapidly and continue growing by riming as graupel and hail. The growth rate of ice hydrometeors exceeds significantly that of an equivalent mass of rain drops (Pinsky et al., 1998). Conversely, in the absence of raindrops, the small cloud drops in strong updrafts can remain liquid up to the homogeneous glaciation level (Rosenfeld and Woodley, 2000). Filaments of nearly adiabatic liquid water content were measured up to the homogeneous freezing temperature of -38°C by aircraft penetrations into feeders of severe hailstorms with updrafts exceeding 40 ms^{-1} (Rosenfeld et al., 2006b). Only very few small ice hydrometeors were observed in these cloud filaments. These feeders of severe hailstorms produced 20 dBZ first echoes at heights of 8-9 km.

An extreme manifestation of strong updrafts with delayed formation of precipitation and homogeneous glaciation is the echo free vault in tornadic and hail storms (Browning and Donaldson, 1963; Browning, 1964; Donaldson, 1970), where the extreme updrafts push the height for the onset of precipitation echoes to above 10 km. However, the clouds that are the subject of main interest here are not those that contain the potential echo free vault, because the vertical microstructure of such clouds is very rarely exposed to the satellite view. It is shown in this study that the feeder clouds to the main storm and adjacent cumulus clouds possess the severe storm satellite retrieved microphysical signature. The parallel to the echo free vault in these clouds is a very high precipitation first echo height, as documented by Rosenfeld et al. (2006b).

Although the role of updraft speed in the vertical growth of cloud drops and onset of precipitation is highlighted, the dominant role of CCN concentrations at cloud base, as has been shown by Andreae et al. (2004), should be kept in mind. Model simulations of rising parcels under different CCN and updraft profiles were conducted by Rosenfeld et al. (2007) to illustrate the respective roles of those two factors in determining the relations between cloud composition, precipitation processes and the updraft velocities. Although the parcel model (Pinsky and Khain, 2002) used in the calculations has 2000 size bins and has accurate representations of nucleation and coalescence processes, being a parcel prevents it from producing realistic widths of drop size distributions due to various cloud base updrafts and supersaturation histories of cloud micro-parcels. Therefore the calculations presented in Rosenfeld et al. (2007) can be viewed only in a relative qualitative sense.

A set of three updraft profiles and four CCN spectra were simulated in the parcel model. Cloud base updraft was set to 2 ms^{-1} for all runs. The maximum simulated drop concentrations just above cloud base were 60, 173, 460 and 1219 cm^{-3} for the four respective CCN spectra. No giant CCN were incorporated, because their addition results in a similar response to the reduction of the number concentrations of the sub-micron CCN, at least when using the same parcel model (see Figure 4 in Rosenfeld et al., 2002). The dependence of activated cloud drop concentration on cloud base updraft speed was simulated with the same parcel model.

According to the calculations, cloud base updraft plays only a secondary role to the CCN in determining the cloud drop number concentrations near cloud base. Further, it was noted that the updraft does not affect the cloud drop size below the height of the onset of coalescence. The height of coalescence onset depends mainly on height and very little on updraft speed. This is so because the coalescence rate is dominated by the size of the cloud drops, which in turn depends only on cloud depth in the diffusional growth zone.

It was found that the updraft speed does affect the height of the onset of significant precipitation (H_R), which was defined as rain water content / cloud water content = 0.1. This was justified by the remarkably consistent relations between CCN concentrations and the vertical evolution of the drop size distribution up to the height of the onset of warm rain (H_R), as documented by Andreae et al. (2004) and Freud et al. (2005). Although the model does not simulate ice processes, these values are still valid qualitatively for vigorous supercooled convective clouds (see for example Figures 7 and 8 in Rosenfeld et al., 2006b), because the main precipitation embryos in such clouds come from the coalescence process, except for clouds with unusually large concentrations of ice nuclei and/or giant CCN. This analysis shows that the vigor of the clouds can be revealed mainly by delaying the precipitation processes to greater heights, and that the sensitivity becomes greater for clouds forming in environments with greater concentrations of small CCN. This being the case, it should be possible to assess the vigor of clouds using multi-spectral satellite imagery to infer cloud microphysical structure.

2.2.2 Satellite inference of vertical microphysical profiles of convective clouds

The vertical evolution of cloud top particle size can be retrieved readily from satellites, using the methodology of Rosenfeld and Lensky (1998) to relate the retrieved effective radius (r_e) to the temperature (T) of the tops of convective clouds. An effective radius > 14 μm indicates precipitating clouds (Rosenfeld and Gutman, 1994). The maximum detectable indicated r_e is 35 μm, due to saturation of the signal. The T-r_e relations are obtained from ensembles of clouds having tops covering a large range of T. This methodology assumes that the T-r_e relations obtained from a snap shot of clouds at various stages of their development equals the T-r_e evolution of the top of an individual cloud as it grows vertically. This assumption was validated by actually tracking such individual cloud elements with a rapid scanning geostationary satellite and comparing with the ensemble cloud properties (Lensky and Rosenfeld, 2006).

Based on the shapes of the T-r_e relations (see Figure 2), Rosenfeld and Lensky (1998) defined the following five microphysical zones in convective clouds:

1) *Diffusional droplet growth zone*: Very slow growth of cloud droplets with depth above cloud base, indicated by shallow slope of dr_e/dT.
2) *Droplet coalescence growth zone*: Large increase of the droplet growth rate dr_e/dT at T warmer than freezing temperatures, indicating rapid cloud-droplet growth with depth above cloud base. Such rapid growth can occur there only by drop coalescence.
3) *Rainout zone*: A zone where r_e remains stable between 20 and 25 μm, probably determined by the maximum drop size that can be sustained by rising air near cloud top, where the larger drops are precipitated to lower elevations and may eventually fall as rain from the cloud base. This zone is so named, because droplet growth by coalescence is balanced by precipitation of the largest drops from cloud top. Therefore, the clouds seem to be raining out much of their water while growing. The radius of the drops that actually rain out from cloud tops is much larger than the indicated r_e of 20-25 μm, being at the upper end of the drop size distribution there.
4) *Mixed phase zone*: A zone of large indicated droplet growth rate, occurring at $T<0^oC$, due to coalescence as well as to mixed phase precipitation formation processes. Therefore, the mixed phase and the coalescence zones are ambiguous at $0<T<-38°C$. The conditions for determining the mixed phase zone within this range are specified in Rosenfeld and Lensky (1998).
5) *Glaciated zone*: A nearly stable zone of r_e having a value greater than that of the rainout zone or the mixed phase zone at $T<0°C$.

All these microphysical zones are defined only for convective cloud elements. Multi-layer clouds start with small r_e at the base of each cloud layer. This can be used to distinguish stratified from convective clouds by their microstructure. Typically, a convective cloud has a larger r_e than a layer cloud at the same height, because the convective cloud is deeper and contains more water in the form of larger drops.

2.3 T-r_e Relations of Severe Convective Storms in Clouds with Small Drops

A microphysically continental cloud is defined as such when CCN concentrations are sufficiently large to induce a drop concentration that is sufficient to suppress drop coalescence and warm rain in the lowest several (2 to 3) km of the cloud. According to Figure 5 in Rosenfeld et al. (2007) this translates to drop concentrations greater than about 400 cm^{-3} near cloud base. Even with small CCN concentrations, a sufficiently low cloud base temperature can always be found such that the diffusional zone of cloud drops in the T-r_e line will extend through the homogeneous glaciation temperature isotherm, even for moderate updraft velocities. This is the case for many of the high plains storms over the western USA, as already noted by Lindsey et al. (2006). This situation is represented schematically by line F of Figure 3B, which illustrates the T-r_e relations under various CCN and updraft scenarios according to the conceptual model.

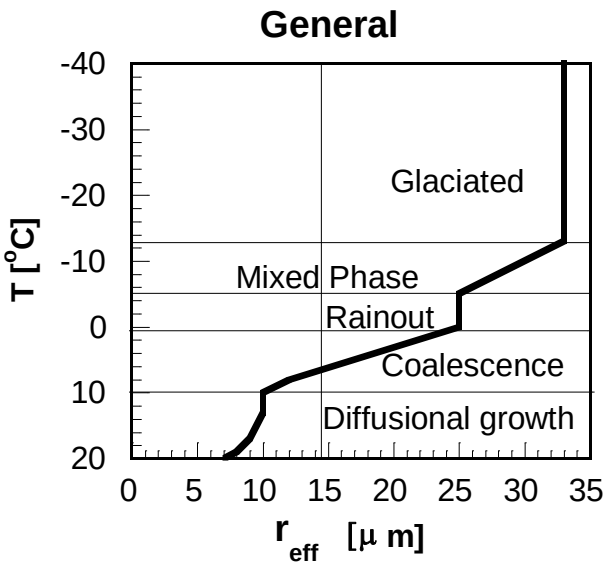

Figure 2: The classification scheme of convective clouds into microphysical zones, according to the shape of the T-r_e relations (after Rosenfeld and Woodley, 2003). The microphysical zones can change considerably between microphysically continental and maritime clouds, as illustrated in Figure 6 of Rosenfeld and Woodley, 2003.

Alternatively, a cloud with an extremely large number of small droplets, such as in a pyro-Cb (See example in Figure 11 of Rosenfeld et al., 2006a), can occur entirely in the diffusional growth zone up to the homogeneous glaciation level even if it does not have very strong updrafts. In any case, a deep (> 3 km) zone of diffusional growth is indicative of microphysically continental clouds, where smaller r_e means greater heights and lower temperatures that are necessary for the transition from diffusional to the mixed phase zone, which is a manifestation of the onset of precipitation. This is demonstrated by the model simulations shown in Figures 4 and 5 in Rosenfeld et al. (2007). Observations of such T-r_e relations in cold and high-base clouds over New Mexico are shown in Figure 1.

Figure 3B illustrates the fact that a highly microphysically continental cloud with a warm base (e.g., >10°C) has a deep zone of diffusional cloud droplet growth even for weak updrafts (line A in Figure 3B and Figure 4a). The onset of precipitation is manifested as the transition to the mixed phase zone, which occurs at progressively greater heights and colder temperatures for clouds with stronger updrafts (line B in Figure 3B and Figure 4b). The glaciation temperature also shifts to greater heights and colder temperatures with increasing updrafts. From the satellite point of view the cloud is determined to be glaciated when the indicated r_e reaches saturation. This occurs when the large ice crystals and hydrometeors dominate the radiative signature of the cloud. Some supercooled water can still exist in such a cloud, but most of the condensates are already in the form of large ice particles that nucleated heterogeneously and grew by riming and fast deposition of water vapor that is in near equilibrium with liquid water. Such was the case documented by Fridland et al. (2004) in convective clouds that ingested mid tropospheric CCN in Florida, where satellite-retrieved T-r_e relations indicated a glaciation temperature of -29°C (not shown).

Further invigoration of the clouds would shift upward the onset of mixed phase and glaciated zones, but glaciation occurs fully and unconditionally at the homogeneous glaciation temperature of -38°C. Any liquid cloud drops that reach to this level freeze homogeneously to same-size ice particles. If most cloud water was not rimed on ice hydrometeors, it would have a radiative impact on the retrieved effective radius and greatly decrease the r_e of the glaciated cloud, as shown in line C of Figure 3B. Yet additional invigoration of the updraft would further shift upward and blur the onset of the precipitation, and reduce the r_e of the

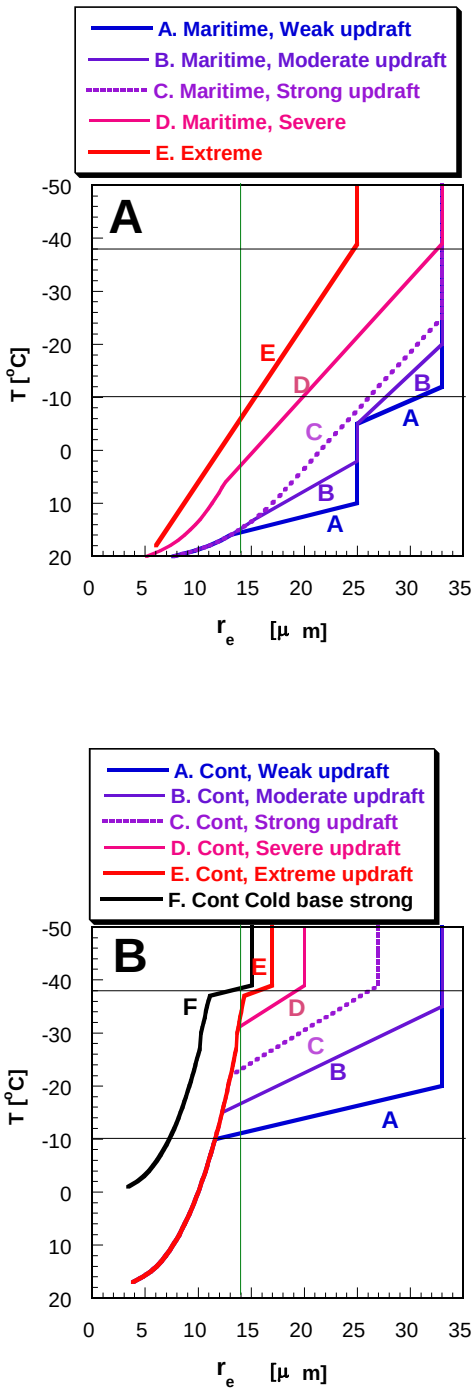

Figure 3: A conceptual model of the way T-r_e relations of convective clouds are affected by enhanced updrafts to extreme values. The vertical green line represents the precipitation threshold of r_e=14 μm (Rosenfeld and Gutman, 1994). The horizontal line at T=-38°C represents the homogeneous freezing isotherm. The left panel is for microphysically maritime clouds with low and warm bases and small concentrations of CCN, and the right panel is for clouds with high CCN concentrations or high and cold bases. In reality most cases occur between these two end types.

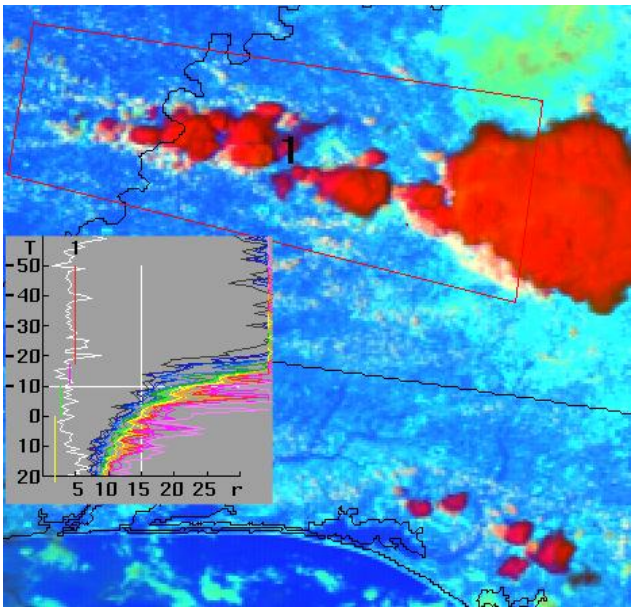

Figure 4a: Same as Figure 1, but for a non-severe convective storm. The image is based on the NOAA-AVHRR overpass on 28 July 1998, 20:24 UTC, over a domain of 232x222 AVHRR 1-km pixels. The cloud system is just to the north of the Florida Panhandle. Note the rapid increase of r_e towards an early glaciation at -17°C. This is case #9855 (see Appendix), with Tbase=20°C, Rbase=8 μm, T14=-5°C, TL=-18°C, dTL=38°C, Tg=-20°C, Rg=33.5μm (See parameter definitions in Figure 5).

glaciated cloud above the -38°C isotherm, until the ultimate case of the most extreme updraft, where the T-r_e profile becomes nearly linear all the way up to the homogeneous freezing level. This situation is illustrated by line E in Figures 3A and 3B and in Figures 4c-4e.

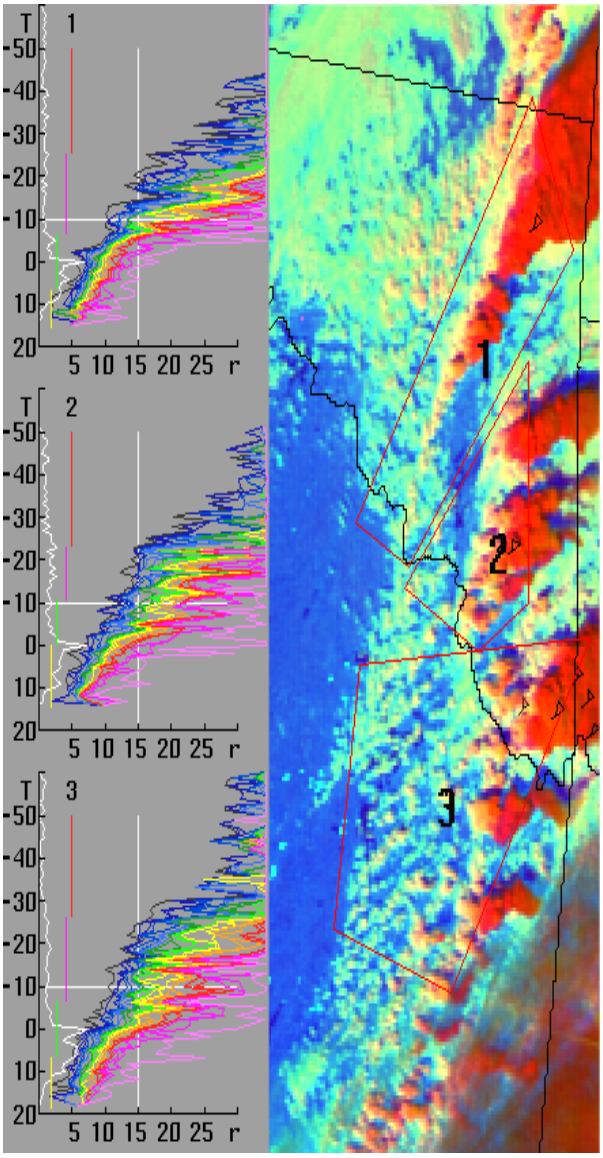

Figure 4b: Same as Figure 1, but for three hail storms. The image is based on the NOAA-AVHRR overpass on 5 March 1999, 21:32 UTC, at a domain of 220x300 AVHRR 1-km pixels. The cloud system is near the eastern border of Oklahoma. The locations of reported hail (0.75-1.75 inch) are marked by small triangles. Note the deep supercooled layer with glaciation temperature of about -25 for the median r_e (denoted by the bottom of the vertical red line), and less than -30°C for the smallest r_e. This is case #9901 with Tbase=8°C, Rbase=5 µm , T14=-12°C, TL=-26°C, dTL=34°C, Tg=-27°C, Rg=32.4 µm (See parameter definitions in Figure 5).

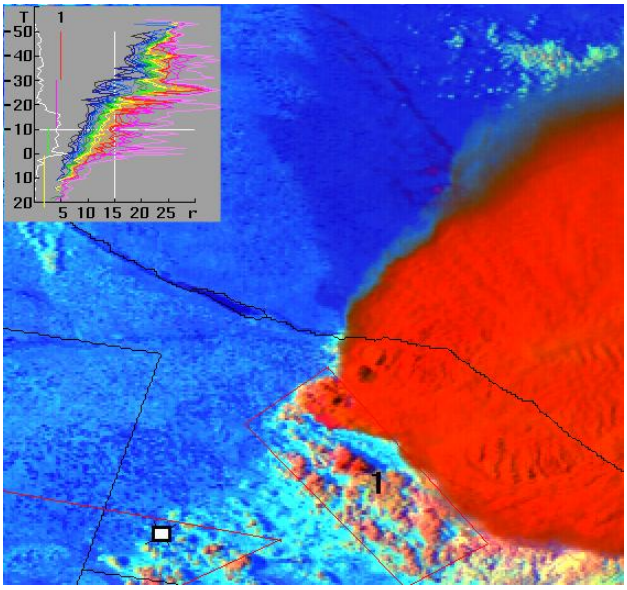

Figure 4c: Same as Figure 1, but for a tornadic storm with 4.5 inch hail. The image is based on the NOAA-AVHRR overpass on 29 June 2000, 22:21 UTC, over a domain of 282x264 AVHRR 1-km pixels. The cloud occurred in southwestern Nebraska. The location of a reported F1 tornado at 23:28 is marked by a rectangle. Note that the tornado occurred in a region that had little cloud development 68 minutes before the tornadic event. This demonstrates that there is predictive value in the cloud field before any of the clouds reach severe stature. A hail swath on the ground can be seen as the dark purple line emerging off the north flank of the storm, oriented NW-SE. Two hail gushes are evident on the swath near the edge of the storm. The precipitation swath appears as darker blue due to the cooler wet ground. Note the linear profile of the T-r_e lines, and the glaciation occurs at the small r_e=25 µm, in spite of the very warm cloud base temperature near 20°C. This is case #0046 with Tbase=8°C, Rbase=5.5 µm, T14=-21°C, TL=-31°C, dTL=39°C, Tg=-32°C,

Rg=20.6 μm (See parameter definitions in Figure 5).

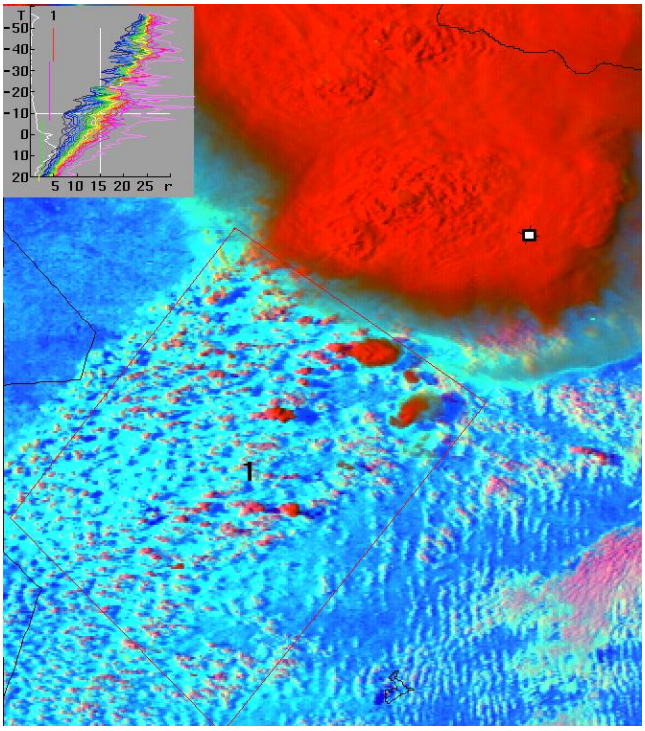

Figure 4d: Same as Figure 1, but for a tornadic storm with 2.5 inch hail. The image is based on the NOAA-AVHRR overpass on 30 April 2000, 22:14 UTC, over a domain of 333x377 AVHRR 1-km pixels. The cloud occurred just to the SE of the Texas panhandle. The location of a reported F3 tornado at 22:40 is marked by a rectangle. Note the very linear profile of the T-r_e lines, and the glaciation occurs at the small r_e=25 μm, in spite of the very warm cloud base temperature of near 20°C, as in Figure 4d. It is particularly noteworthy that this T-r_e is based on clouds that occurred ahead of the main storm into an area through which the storm propagated. The same is indicated in Fig. 8d, but to a somewhat lesser extent. This is case #0018 with Tbase=18°C, Rbase=4.4 μm, T14=-15°C, TL=-37°C, dTL=55°C, Tg=-38°C, Rg=23.9 μm (See parameter definitions in Fig. 5).

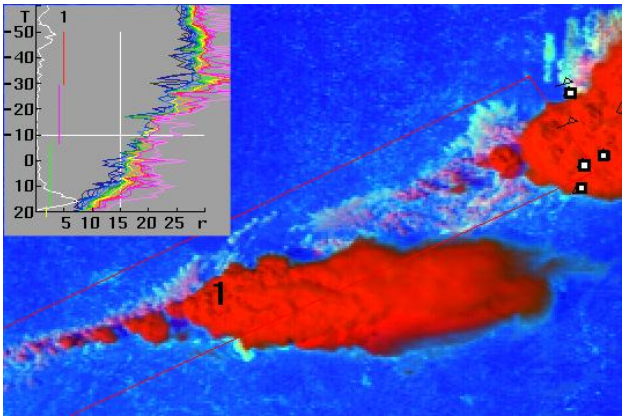

Figure 4e: Same as Figure 1, but for a tornadic storm with 1.75 inch hail. The image is based on the NOAA-AVHRR overpass on 20 July 1998, 20:12 UTC, over a domain of 262x178 AVHRR 1-km pixels. The cloud occurred in NW Wisconsin. The locations of reported F0 tornadoes are marked by rectangles. Note the large r_e at the lower levels, indicating microphysically maritime microstructure, followed by a very deep mixed phase zone. Very strong updrafts should exist for maintaining such a deep mixed phase zone in a microphysically maritime cloud, as illustrated in line C of Fig. 3A. This is case #9847 with Tbase=16°C, Rbase=8 μm, T14=8°C, TL=-31°C, dTL=47°C, Tg=-32°C, Rg=27.8 μm (See parameter definitions in Fig. 5).

2.4 T-r_e Relations of Severe Convective Storms in Clouds with Large Drops

Line A in Fig. 3A is similar to the scheme shown in Fig. 2, where a microphysically maritime cloud with weak updrafts develops warm rain quickly and a rainout zone, followed by a shallow mixed phase zone. When strengthening the updraft

(line B), the time that is needed for the cloud drops in the faster rising cloud parcel to coalesce into warm rain is increased. Consequently, the rainout zone is reached at a greater height, but the onset of the mixed phase zone is anchored to the slightly supercooled temperature of about -5°C. This decreases the depth of the rainout zone. The greater updrafts push the glaciation level to colder temperatures. Additional invigoration of the updraft (line C) eliminates the rainout zone altogether and further decreases the glaciation temperature, thus creating a linear T-r_e line up to the glaciation temperature. Even greater updrafts decrease the rate of increase of r_e with decreasing T, so that the glaciation temperature is reached at even lower temperatures. It takes an extreme updraft to drive the glaciation temperature to the homogeneous glaciation level, as shown in lines D and observed in Fig. 4f.

Most cases in reality occur between the two end types that are illustrated schematically in Fig. 3. Examples of T-r_e lines for benign, hailing and tornadic convective storms are provided in Fig. 4. It is remarkable that the T-r_e relations occur not only in the feeders of the main clouds, but also in the smaller convective towers in the area from which the main storms appear to propagate (see Figures 4e and 4f). This does not imply that the smaller convective towers and the upshear feeders have updraft speeds similar to the main storms, because these core updrafts at the mature stage of the storms are typically obscured from the satellite view. However, it does suggest that the satellite inferred updraft-related microstructure of those smaller clouds and feeders is correlated with the vigor of the main updraft. This has implications for forecasting, because the potential for severe storms can be revealed already by the small isolated clouds that grow in an environment that is prone to severe convective storms when the clouds are organized.

Based on the physical considerations above it can be generalized that a greater updraft is manifested as a combination of the following trends in observable T-r_e features:

- Glaciation temperature is reached at a lower temperature;
- A linear T-r_e line occurs for a greater temperature interval;
- The r_e of the cloud at its glaciation temperature is smaller.

These criteria can be used to identify clouds with sufficiently strong updrafts to possess a significant risk of large hail and tornadoes. The feasibility of this application is examined in the next section.

2.5 The Roles of Vertical Growth Rate and Wind Shear in Measuring T-r_e Relations

Severe convective storms often have updrafts exceeding 30 ms^{-1}. At this rate the air rises 9 km within 5 minutes. The tops form anvils that diverge quickly, and without strong wind shear the anvil obscures the new feeders to the convective storm, leaving a relatively small chance for the satellite snap shot to capture the exposed tops of the vigorously growing convective towers. Therefore, in a highly unstable environment with little wind shear the T-r_e relations are based on the newly growing storms and on the cumulus field away from the mature anviled storms. An example of moderate intensity little-sheared convection is shown in Fig. 4a.

When strong wind shear is added, only strong and well organized updrafts can grow into tall convective elements that are not sheared apart. The convective towers are tilted and provide the satellite an opportunity

to view from above their sloping tops and the vertical evolution of their T-r_e relations (see examples in Figs. 4b and 4d). In some cases the strong divergence aloft produces an anvil that obscures the upshear slope of the feeders from the satellite view. Yet unorganized convective clouds that often pop up in the highly unstable air mass into which the storm is propagating manage to grow to a considerable height through the highly sheared environment and provide the satellite view necessary to derive their T-r_e relations. Interestingly and importantly, the T-r_e relations of these pre-storm clouds already possess the severe storm microphysical signature, as evident in Fig. 4e. Without the strong instability these deep convective elements would not be able to form in strong wind shear. Furthermore, often some of the horizontal momentum diverts to vertical in a sheared convective environment. Weisman and Klemp (1984) , modeling convective storms in different conditions of vertical wind shear with directional variations, showed that updraft velocity is dependent on updraft buoyancy and vertical wind shear. In strong shear conditions the updrafts of long-lived simulated supercell storms interacted with the vertical wind shear and this interaction resulted in a contribution of up to 60% of the updraft strength. Furthermore, Brooks and Wilhelmson (1990) showed, from numerical modeling experiments, an increased peak updraft speed with increasing helicity. Therefore, to the extent that wind shear and helicity enhance the updrafts, the severe storm microphysical signature inherently takes this into account.

2.6 The Potential Use of the T-r_e Relations for the Nowcasting of Severe Weather

2.6.1 Parameterization of the T-r_e relations

The next step was the quantitative examination of additional cases, taken from AVHRR overpasses that occurred 0-75 minutes before the time of tornadoes and/or large hail in their viewing area anywhere between the US east coast and the foothills of the Rocky Mountains. The reports of the severe storms were obtained from the National Climate Data Center (http://www4.ncdc.noaa.gov/cgi-win/wwcgi.dll?wwEvent~Storms). For serving as control cases, visibly well defined non-severe storms (i.e., without reported tornado or large hail) were selected at random from the AVHRR viewing areas. These control cases were selected from the viewing area of the same AVHRR overpasses that included the severe convective storms at distances of at least 250 km away from the area of reported severe storms. The relatively early overpass time of the AVHRR with respect to the diurnal cycle of severe convective storms allowed only a relatively small dataset from the years 1991-2001, the period in which the NOAA polar orbiting satellites drifted to the mid and late afternoon hours. Unfortunately this important time slot has been neglected since that time. In all, the dataset includes 28 cases with tornadoes and hail, 6 with tornadoes and no hail, 24 with hail only and 38 with thunderstorms but no severe weather. The case total was 96. The total dataset is given in Appendix A of Rosenfeld et al. (2007).

The AVHRR imagery for these cases was processed to produce the T-r_e relations, using the methodology of Rosenfeld and Lensky (1998). The T-r_e functions were parameterized using a computerized algorithm into the following parameters, as illustrated in Fig. 5:

Tbase: Temperature of cloud base, which is approximated by the warmest point of the T-r_e relation.

Rbase: The r_e at cloud base.
T14: Temperature where r_e crosses the precipitation threshold of 14 um.
TL: Temperature where the linearity of the T-r_e relation ends upwards.
DTL: Temperature interval of the linear part of the T-r_e relation. Tbase - TL
Tg: Onset temperature of the glaciated zone.
Rg: r_e at Tg.

These parameters provide the satellite inferences of cloud-base temperature, the effective radius at cloud base, the temperature at which the effective radius reached the precipitation threshold of 14 μm, the temperature at the top of the linear droplet growth line and the temperature at which glaciation was complete. The T-r_e part of the cloud which is dominated by diffusional growth appears linear, because the non linear part near cloud base is truncated due to the inability of the satellite to measure the composition of very shallow parts of the clouds. The T-r_e continues to be linear to greater heights and lower temperatures for more vigorous clouds, as shown schematically in Fig. 3.

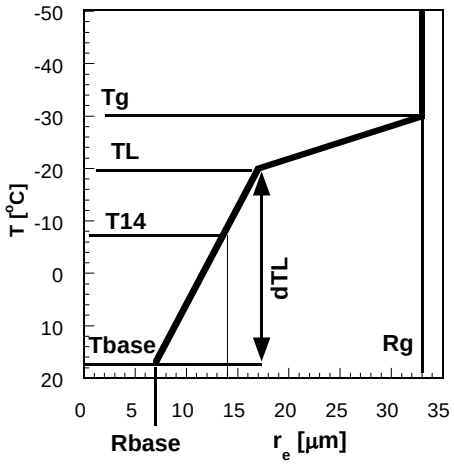

Fig. 5: Illustration of the meaning of the parameters describing the T-r_e relations.

These parameters were retrieved for various percentiles of the r_e for a given T. The r_e at a given T increases with the maturation of the cloud or with slower updrafts, especially above the height for the onset of precipitation, as evident in Fig. 1. Therefore, characterization of the growing stages of the most vigorous clouds in percentiles requires using the small end of the distribution of r_e for any given T. In order to avoid spurious values, the 15th percentile and not the lowest was selected for the subsequent analyses. The 15th percentile was used because it represents the young and most vigorously growing convective elements, whereas larger percentiles represent more mature cloud elements.

The mean results by parameter and by storm type were tabulated by Rosenfeld et al. (2007). According to the tabulations, the likelihood of a tornado is greater for a colder top of the linear zone and for a colder glaciation temperature. In extreme cases such as that shown in Fig. 4e there is little difference between Tg and TL because of what must have been violent updrafts. In addition, smaller effective radius at cloud base indicates higher probability for a tornadic event.

2.6.2 Statistical evaluation using AVHRR

The primary goal of the initial analyses making use of AVHRR polar-orbiter imagery was to determine whether the probability of a tornado or hail event might be quantified using the parameterized values of satellite retrieved T-r_e relations of a given field of convective clouds. Doing this involved the use of binary logistic regression (Madalla, 1983), which is a methodology that provides the probability of the occurrence of one out of two possible events.

If the probability of the occurrence of a tornado event is P, the probability for a non-tornado is 1-P. Given predictors X1, X2,… Xi, the probability P of the tornado is calculated using binary logistic regression with the predictors as continuous, independent, input variables using equation (3):

$$\ln\left(\frac{P}{1-P}\right) = \alpha + \beta x \quad (3)$$

The basic model is similar in form to linear regression model (Note the right side of the equation.), where α is the model constant and β is a coefficient of the parameter x of the model.

The first step is calculation of P/(1-P) according to (3). The logistic regression was done in a stepwise fashion, so that the procedure was allowed to select the parameters that had the best predictive skill. The details of the calculations are given in Rosenfeld et al. (2007). The analysis revealed that microphysical continentality along with slow vertical development of precipitation in the clouds apparently are essential for the formation of tornadoes. Also non-tornadic hail storms can be distinguished from non severe storms by their microphysically continental nature, as manifested by smaller Rbase and cooler cloud bases. However, the tornadoes differ mostly from hail-only storms by having smaller r_e aloft (lower T14), extending the linear part of the T-r_e relations to greater heights (greater dTL) and glaciating at lower temperatures that often approach the homogeneous freezing isotherm of -38°C (lower Tg). The freezing occurs at smaller r_e (lower Rg). All this is consistent with the conceptual model that is illustrated in Fig. 3.

3.0 INITIAL TESTS OF THE CONCEPTS USING GOES IMAGERY (SBIR 1)

The initial investigation discussed above, suggested that multi-spectral, polar-orbiter, AVHRR satellite imagery could be used to identify clouds that had the potential to produce severe weather. This finding would have positive ramifications for severe weather forecasting and warning if multi-spectral Geostationary Operational Environmental Satellite (GOES) imagery, providing good temporal resolution, could be used for the measurements. At this point Dr. Woodley contacted NOAA's Small Business Innovative Research (SBIR) program to seek support to test the feasibility of the concept as applied to GOES imagery. The goal of this SBIR Phase 1 effort would be to determine whether GOES multi-spectral satellite imagery has potential for the short-term forecasting of severe weather, especially tornadoes. It would be predicated on the finding from initial analyses of multi-spectral polar-orbiter satellite data (described herein) that the height profiles of cloud-particle effective radius, showing a deep zone of diffusion droplet growth, little coalescence, no precipitation, and delayed glaciation to near the temperature of homogeneous nucleation (~ -38^{o}C) are associated with tornadoes and hail. This would mean that a satellite-based severe storm signature is an extensive property of the clouds before storm outbreaks. It implied further that the probabilities of tornadoes and large hail might be obtained at lead times > 1 hour prior to the actual event. This would represent a major improvement over what is possible currently. Because of these potential payoffs, Woodley Weather Consultants received a SBIR Phase 1 (SBIR-1) award to test these concepts on GOES imagery.

In making use of GOES instead of AVHRR satellite data it was necessary to trade the fine (1-km) spatial resolution

obtainable from the polar orbiters once-per-day for the degraded 4-km spatial resolution that is available in GOES multi-spectral images every 15 to 30 minutes. Upon comparing the two imagery sources, the GOES data did not seem to have a systematic error relative to the polar-orbiter AVHRR data. The main effect was losing the smaller sub-pixel cloud elements, which were primarily the lower and smaller clouds. Therefore, cloud base temperature could not be relied on quantitatively as in the AVHRR imagery, so that it would be necessary to divide the GOES scenes into two indicated cloud base temperature classes with a demarcation at 15°C. The effectiveness of the detection of linearity of the profiles and glaciation temperature was compromised to a lesser extent, because the cloud elements were already larger than the pixel size when reaching the heights of the highly supercooled temperatures. No quantitative assessment of the effect of the resolution was done in this preliminary study beyond merely testing the skill of the T-r_e retrieved parameters.

The analysis using GOES imagery was done only for detecting tornadoes, because the AVHRR analysis showed that the predictor parameters had more extreme values for tornadoes than for hail. The continuing research entailed the use of archived multi-spectral GOES imagery instead of polar-orbiter satellite data, which were used to derive the relationships. All of the useable old polar-orbiter data had been exhausted during the initial tests and there is no prospect of additional useable polar-orbiter data due to the oversight of lack of a late afternoon slot for the polar orbiters. Further, imagery from a polar orbiting satellite is available at a given location only once or twice per day, which is too infrequent for forecasting purposes. Thus, the key question going into SBIR-1 effort was whether anything meaningful could be obtained by using the GOES imagery that provides much-enhanced temporal resolution at the expense of the spatial resolution.

Seventeen (17) days with past tornadic events were examined using conventional weather data and archived, multi-spectral, GOES-10 imagery, which were obtained from the Cooperative Institute for Research in the Atmosphere (CIRA) satellite archive. For each case, the area of interest was first identified by noting severe weather reports from the Storm Prediction Center's (SPC) website. The chosen area typically encompassed at least 6 central U.S. states, but was larger for the more extensive severe weather outbreaks. Data were obtained beginning in the morning, usually around 1600 UTC, and extended to near sunset. Rapid scan imagery was not analyzed, and only the regular 15 to 30 minute scans were used. The GOES satellite imagery was analyzed using the T-r_e profiles for multiple significant convective areas within the field of view. The T-r_e parameters as defined in Fig. 5 were calculated for each such convective area. The GOES-retrieved r_e reached saturation at 40 μm, instead of 35 μm for the AVHRR. Other than that the T-r_e parameters were calculated similarly.

On the 17 case days there were 86 analyzed convective areas, 37 of the 86 analyzed areas had a total of 78 tornadoes. As in the analysis of the AVHRR data set, logistic regression was done in a stepwise fashion, so that the procedure was allowed to select the parameters that had the best predictive skill. The satellite-based predictors were found to be at least as good as the sounding-based predictors, although the two are only loosely correlated. The logistic regression parameters and coefficients data for the soundings and satellite retrieved parameters are in Rosenfeld et al. (2007).

The graphical representation of the probability (P) for a tornado is depicted best by the transformation of P to log10(P/(1-P)). This transformation of P is used in the graphical display shown in Figure 6 because it is important to expand the scales near P=0 and P=1. Note that when log10(P/(1-P) = 0, P = 0.50. Histograms of $\log_{10}(P/(1-P))$ for the satellite-based logistic regression prediction models are shown in Figure 7. The top panel gives the satellite-based predictions for tornadic and non-tornadic storms, while the bottom panel gives the sounding-based predictions for tornadic and non-tornadic storms. The regression predictions provide good separation for the cases.

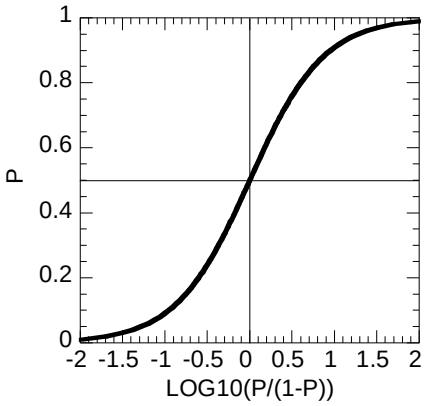

Figure 6: The relations between the probability for an event P and the transformation to log10(P/(1-P)).

The potential lead time from the geostationary satellite data for a severe weather event was assessed by Rosenfeld et al. (2007) for some of the most intense tornadoes in the data set. The satellite-based predictor rose some 90 minutes or even more before the actual occurrence of the tornado. In many cases it manifested itself with the first clouds that reached the glaciation level. For all the tornadic storms in the dataset the tornado probabilities exceeded 0.5 by 150 minutes before the occurrence of the tornado, and increased to 0.7 at a lead time of 90 minutes. In comparison, the median P of the non-tornadic storms was about 0.06. This shows the great "Early-Alert" potential of the methodology.

The overall predictive skill of the soundings and the GOES satellite are comparable, but the satellite is much more focused in time and space. The difference between the sounding and satellite based predictions can be better understood when plotting the time dependent predictors for tornadic cases. The sounding based predictor is fixed in time and space for the analyzed area, because there is only one relevant sounding that can indicate the pre-storm environment before the convective overturning masks it. The satellite predictor on the other hand varies and is recalculated independently for each new satellite observation. This allows the satellite based predictor to react to what the clouds are actually doing as a function of time at scales that are not resolved properly by the soundings or by models such as the Rapid Update Cycle (RUC).

The association between strong updrafts, as inferred by the T-r_e profiles, and tornadoes and hailstorms makes sense physically. The combined physical considerations and preliminary statistical results suggest that clouds with extreme updrafts and small effective radii are highly likely to produce tornadoes and large hail, although the strength and direction of the wind shear probably would be major modulating factors. The generation of tornadoes often (but not always) requires strong wind shear in the lowest 6 km and low level helicity (Davis, 2006). According to the satellite inferences here this might be helping spin up the tornadoes in storms with very strong and deep updrafts that reach the anvil level. These strong updrafts aloft are

revealed by the linear T-r_e profiles that extend to greater heights and r_e reaching smaller values at the -38°C isotherm in tornadic versus hail storms. These inferred stronger and deeper updrafts in tornadic storms compared to hailstorms imply that in low CAPE and high shear environment some of the energy for the updrafts comes from converting horizontal to vertical momentum, as already shown by Browning (1964). Fortuitously, the tilting of the feeder and pre-storm clouds in the high shear tornadic storms render them easier to see by satellite and this facilitates the derivation of the T-r_e profiles and the retrieval of tornadic microphysical signatures, as described above.

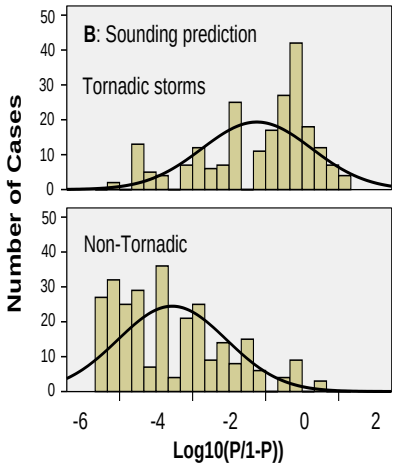

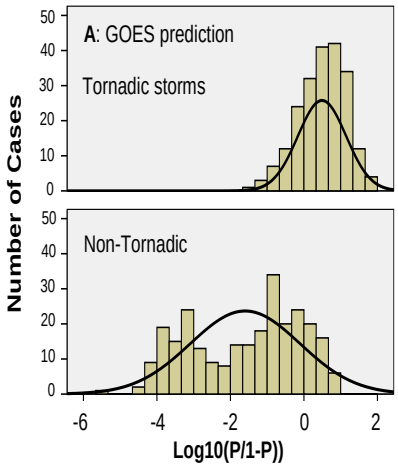

Figure 7: Histograms of the predictions $\log_{10}(P/(1-P))$ for the GOES satellite (A) and the sounding (B) based models. The upper panel is for tornadic scenes, and the lower panel for non tornadic areas.

The research to this point had indicated that the potential of new growing deep convective clouds to become storms that produce large hail and tornadoes can be revealed by the satellite-retrieved vertical evolution of the microstructure of these clouds. Deep clouds composed of small drops in their lower parts and cool bases are likely to produce hail, because such clouds produce little warm rain and most of the condensate becomes supercooled water with relatively small concentrations of precipitation embryos. Large graupel and small hail can develop under such conditions. The hail becomes larger with greater updraft velocities at the supercooled levels. This can be inferred by the increased depth of the supercooled zone of the clouds, as indicated by lower glaciation

temperatures. This is also manifested by an increase of the height for onset of significant precipitation, as indicated by lower T14. Tornadic storms, which are often accompanied by very large hail, are characterized by the parameters that indicate the strongest updrafts at the supercooled levels, which are indicated by markedly lower values of Tg and TL and smaller Rg than for hail-only storms.

This study did not address the role of wind shear in tornado development. However, the extent that wind shear modulates severe storms by affecting their updraft speeds can be revealed by the methodology presented in this study. The helicity of the wind shear should increase the probability of a tornado for a given updraft velocity (Weisman and Klemp, 1984; Brooks and Wilhelmson 1990; Rasmussen and Blanchard, 1998). A combination of the satellite methodology with soundings parameters should be more powerful than each method alone. The sounding and synoptic parameters identify the general areas at risk of severe weather and the continuous multispectral satellite imagery identifies when and where that risk is about to be realized.

This study suggests that multispectral satellite data have yet untapped predictive skill for nowcasting of hail and mainly tornadic storms. This application will require using retrieved microstructure from geostationary satellites, which provide smaller spatial resolution (3 to 4 km at the sub geostationary satellite point) than the polar-orbiting satellites used in this study (1.1 km beneath the satellite) and are hence less useful. However, the added dimension of time evolution that is possible with GOES imagery appears to compensate for its poorer spatial resolution, and allows timely early alerts of the risk of tornadoes from the developing storm clouds. While this method appears to have useful results with the current GOES satellites, it is developed with the expectation of improved resolution with the next generation of geostationary satellites. The resolution will be 2 km for the GOES-R and 1-km for the high resolution coverage of the METEOSAT third generation.

SBIR-1 had not been aimed at testing an operational methodology for satellite quantification of the risks of severe convective storms, but rather the testing of the validity of the conceptual model that will hopefully allow subsequent development of such an operational methodology using geostationary satellites. Therefore, the statistical analyses are exploratory in nature at this stage of the research. Although the small sample size does not allow a rigorous evaluation of the predictive skill of the conceptual model, it is sufficient to support the conceptual model. The existence of the severe storm signature in the pre-storm clouds provides us with the prospect that this methodology, when applied to geostationary multispectral satellite imagery, will make it possible to identify earlier than is possible now developing cloud areas that are about to become severe convective storms, possibly producing tornadoes and large hail. The clouds in this early stage typically have not yet developed radar severe storm signatures. Therefore, the capability of detecting the potential of clouds to become severe convective storms may provide additional lead time for more focused “watch” areas, although with lesser accuracy and focus than the detection of severe weather that is already possible with radar. This method has the potential of filling the currently large gap between large, poorly focused “watch” areas and "warnings" by providing “Early Alerts” of severe convective storms that are actually observed subsequently. The challenge that the National Weather Service faces in

coping with the severe weather threat is addressed in the next section.

4.0 COPING CURRENTLY WITH THE SEVERE WEATHER THREAT

Statistics from the Storm Prediction Center show that over 1,000 tornadoes strike the United States each year, making it the most tornado-prone country in the world. Up to 40 deaths per year have occurred in the U.S. alone over the past 10 years. The most notable of the tornadic events was the series of tornadoes that struck the Oklahoma City area on May 3, 1999. These were the most damaging in U.S. history, causing over 1 billion dollars in damage and completely destroying over 2,500 structures. Although lives were lost in these events, excellent warnings from the National Weather Service saved many lives. Even so, NWS forecasts need to be improved further especially as it relates to "false alarms." How this can be done was addressed by the SBIR Phase 2 research. Before getting into that it is important to put everything into the context of current NWS tools and procedures.

After completion of NWS' Modernization during the l990's, it moved from a tiered office structure of 320 full-time and part-time local NWS offices to a structure with about 122 modernized, full-time weather forecast offices (WFOs—for further details on the NWS Modernization, see Friday (l994). Each office is fully equipped with the latest technologies for observing, forecasting, and warning of severe thunderstorms and their attendant hazardous phenomena, such as tornadoes, large hail, heavy rain, and high winds or "downbursts." The key new technologies now implemented nationwide as part of NWS Modernization include WSR-88D Doppler weather radar (a network of 165 radars run collaboratively by the NWS, DoD, and DoT), Automated Surface Observing Systems (ASOS) at over 1,200 sites, GOES-10 and 12 (the new generation, with greater spatial resolution, more frequent imaging, and more image channels, including multi-spectral data), and most important, the Automated Weather Interactive Processing System (AWIPS) {one at each WFO and several additional at each of the National Centers for Environmental Prediction (NCEP, including SPC) and River Forecast Centers}. AWIPS is a computer workstation and display system and is crucial to integrating the vast amount of data that flows from WSR-88D, ASOS, GOES-10 and 12, wind profilers, and other present and planned observing systems (e.g., NPOESS). See also Smith et al., (1999), and Wilson et. al, (1999) for more details. AWIPS also provides the computer and communications power to prepare short-term forecasts and warnings of all hazardous weather, especially severe thunderstorms and tornadoes.

Tornado prediction has improved dramatically over the past 25 years. This is attributable to the continuous, high resolution coverage of GOES satellites; improved use of radar, forecaster training, and local storm spotter networks, and awareness campaigns.

The conceptual models on how tornadoes form have evolved from a simple, random bathtub vortex approach to one where a parent circulation, termed a mesocyclone, sometimes develops at midlevels in a severe supercell thunderstorm prior to tornado touchdown. However, the l994-95 Project VORTEX (Rasmussen et al, l994) has found that large, intense tornadoes may spin-up in the boundary layer initially without any mesocyclone in the parent storm.

The newer ETA (now NAM) and rapid update cycle (RUC) mesoscale models

being run at NCEP are providing severe storm forecasters with higher resolution and more accurate predicted fields of the critical atmospheric parameters that lead to severe thunderstorm and tornado development. These models can also be used to portray forecasted atmospheric soundings at any location out to 48 hrs. Moreover, the new Weather and Research Forecast Model (WRF) is being tested in real-time at resolutions down to 4-10 km, and shows remarkable skill in some tornadic storm-development scenarios. The WRF is now running operationally at NCEP as the NAM Model at 13 km resolution.

There have also been significant improvements in warning for tornadoes over the past 25 years. In l978, the probability of detection (POD) score for tornadoes for NWS was only 0.22. In other words, 22% of the tornadoes had warnings that preceded their initial impacts. Warning lead-times averaged just 3 min before impact. In l998, the POD for tornado warnings had risen to 0.65. The average lead-time for those events that had a prior tornado warning was 11 min. The major factor in this increase is the installation and skilled use of the WSR-88D radars during the 1990's and early 21st Century. However, the false alarm ratio in recent years has risen to a national average of about 0.75. *The total number nationally of severe thunderstorm and tornado warnings has also risen to 10,000-12,000 per year*. This means that while forecasters are doing a better job in detecting and warning about tornadoes with greater lead-times, they are issuing warnings too often and appear to be over warning the public. This could cause problems later with public credibility and response (Golden and Adams, 2000); however, the extent to which high false alarm ratios influence warning response behavior has not been systematically researched by social scientists. NWS seems to be moving from the era of "detected" warnings (warnings based on detecting existing tornadoes) to the era of "predictive" warnings (warnings based on forecasts of tornado formation). Generating such predictive warnings is the essence of the SBIR Phase 2 (SBIR-2) research effort. This, combined with improvements in warning coordination and communication, has lead to the reduction in morbidity and mortality for tornadoes. Continued improvement is expected.

The tornado information communication paradigm used by NWS includes several types of forecast and warning products. Outlooks for severe convective weather (i.e., severe thunderstorms) are issued 1-2 days in advance from SPC. An example of a convective weather outlook for May 10, 2008, a day of interest in the Oklahoma tests of the methodology, is given in Figure 8. The storm reports for this day, which were available the following morning, are given in Figure 9. The reports of severe weather agreed well with the convective outlook for this day.

The convective outlooks are the first notifications of the threat to both local NWS offices and local emergency management officials. These outlooks may be followed by the issuance of tornado watches that are issued currently for large areas that have a significant potential to experience severe thunderstorms capable of producing tornadoes. This is the first official notification to the public of a significant threat. The SPC watch process is discussed in more detail below. Shorter range outlooks are issued in the morning during tornado season by local NWS offices to describe the likelihood of severe weather in their forecast areas. This includes information on type of severe weather, general locations within a county warning area, and time frames. As events unfold, short-term forecasts are issued on a frequent

"as needed" basis as the severe weather begins to form. When a tornado is believed to be imminent, based on radar or other detection technology, or is spotted and reported, a tornado warning is issued. The warning contains specific language on areas at risk, time frames, specific hazards, recommended protective behavior for those at risk, and the office issuing the warning. It is also important to note that NWS' approach to the warning process for tornadoes is a weather-warning partnership with local emergency managers, private forecasters and the news media. The SBIR-2 tests fit nicely into this scenario.

The proposed multi-spectral satellite tornado detection and warning technique is highly complementary to other sources of data used both in SPC's tornado watches and WFOs' tornado warnings. In the former, SPC typically issues tornado watches based on mesoscale diagnostic and analysis products, as well as NWP model data, especially the RUC and NAM. Tornado watches are now typically 24,000 sq mi in size (see Table 1) and last for 6-8 hours. Of great interest is the fact that only slightly more than half of all tornado watches are verified by at least one tornado subsequently within them; moreover, only slightly more than half of all reported tornadoes fall within a tornado watch. There is clearly much opportunity for improvement in tornado watches. However, SPC does a much better job of catching *significant tornadoes* within one of their tornado watch areas (79%). Finally, about 90% of all reported tornadoes fall within either a severe thunderstorm or a tornado watch.

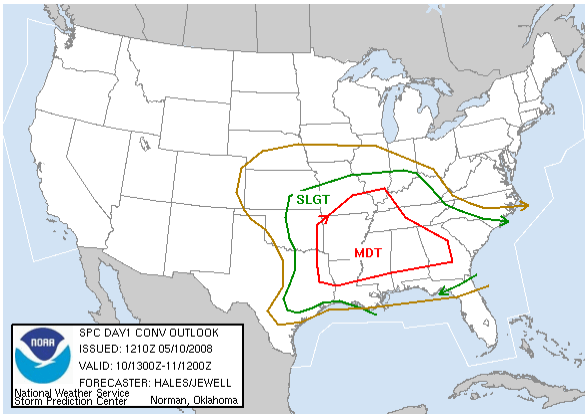

Figure 8. The convective weather outlook for the United States on May 10, 2008 issued by the Storm Prediction Center (SPC)

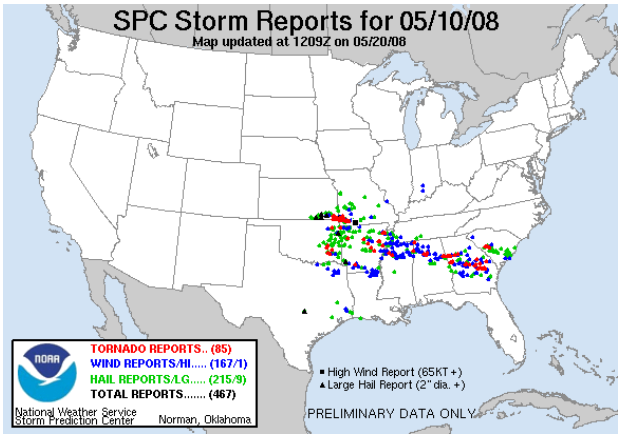

Figure 9. The SPC Storm Reports for May 10, 2008 as updated on May 20, 2008.

The lead-time on some tornado watches is sometimes only about one-half hour. Thus, if delivery of multi-spectral satellite data can be made timelier, it should contribute to increased lead-time of tornado watches, as well as higher skill in capturing tornadoes within watch areas. It should also contribute to more accurate "convective outlook" products issued during each morning by SPC to indicate risk areas of severe weather over the entire U.S. (especially for those tornado outbreak cases when supercells are developing explosively and early).

One good example of prototype technologies that have improved warning issuance is the Warning Decision Support System (WDSS), developed by Eilts and colleagues at NOAA's National Severe Storms Laboratory (Eilts, l997; Johnson et al., l997). It was developed to meet the needs of forecasters in WFO's to help them make timely, effective, and efficient warning decisions (for severe weather, tornadoes and flash floods). WDSS is a combination of a number of automated algorithms that utilize Doppler radar data to automatically detect and predict severe weather phenomena, and an innovative color display that was designed specifically to meet the needs of weather forecasters. The severe weather detection and prediction algorithms utilize image processing, artificial intelligence, neural networks, expert system, and fuzzy logic techniques to detect weather phenomena and to predict the occurrence of severe weather at the surface 0-30 min in advance.

WDSS was extensively field tested at several NWS field offices over the latter half of the l990's. It was also selected to support the l996 Summer Olympics in Atlanta. Most important, the WDSS system was deployed and used by the Oklahoma City, OK forecasters during the massive May 3, 1999 Central Oklahoma tornado outbreak. During that outbreak, the OKC WFO issued 116 separate warnings with better-than-average lead-times of 20-60 min. The OKC Meteorologist-in-Charge credited the warnings' success and relatively low number of fatalities to four major system components: (1) The WSR-88D radar network; (2) the new AWIPS, especially its warning generation software; (3) WDSS used as an adjunct to AWIPS; (4) the close coordination among WFOs, local media, and local/state emergency management offices. We should also note that key WDSS functionality has subsequently been incorporated into the AWIPS systems at WFOs nationwide, primarily though the SCAN (System for Convection Analysis and Nowcasting--Smith et. al, l999) program.

Thus, there is a precedent for the development and use of prototype technologies to improve severe weather forecasts. This is the goal of SBIR- 2 for much of the United States, including those areas that rarely experience tornadoes such as that west of the Rocky Mountains. Some of the cases analyzed in SBIR-1 were over the Rockies and Western U.S., where NEXRAD coverage is sparse and the radar antennas are at high elevations above cloud base. The technique also seems to have superior skill over NEXRAD alone in those cases when the NEXRAD didn't detect any mesocyclones in the parent storm. The Salt Lake City, Eastern Wyoming and Colorado cases show great promise in improving tornado warning skill (PODs and lead-times) and reducing the current high false-alarm rate for warnings based primarily on NEXRAD. Somewhat surprisingly, the technique demonstrates skill in forecasting those storms about to produce even weak to moderate tornadoes (F0-F2's), and it can anticipate both small numbers of tornadoes as well as major outbreaks. Nationally, the False-Alarm-Rate for all tornado warnings still averages about 75%, and there has been a disconcerting decrease in the POD during the past year.

It now must be shown in SBIR-2 how the technique can be automated to produce useful near-real-time products for the SPC and WFO forecasters to use as a complement to their other operational tools.

TABLE 1: SPC Tornado Watch Statistics (averaged over ten years, l995-2004)

57% - Tornado watches verified by a tornado
92% - Thunderstorm and tornado watches verified by either a severe thunderstorm or tornado report
54% - Tornadoes in a tornado watch
79% - Significant tornadoes in a tornado watch
71% - Tornadoes in either a tornado or severe thunderstorm watch
90% - Significant tornadoes in either a tornado or severe Thunderstorm watch

79% - Significant tornadoes (F2-F5) in a tornado watch
60% - Severe thunderstorm or tornado in either a severe thunderstorm or tornado watch
72% - Significant Severe Thunderstorm (hail>2",Gust>) or significant tornado in tornado or severe thunderstorm watch
23,773 mi^2 - median area tornado watch
22,967 mi^2 - median area tornado and severe thunderstorm watches

These are all 10 year averages (1995-2004) of the parameters computed for each individual year. Lead time is from the time a watch is publicly issued to the first event within the watch. It must be remembered that there is a coordination period, usually of about 17 minutes, between the time the decision to issue a watch is made and the time the watch is publicly issued. Since follow-on watches (i.e., those over downstream areas immediately adjacent to the watch) are included in the lead time computations, these numbers are really low estimates.

Starting in 2005, SPC began verifying watches by individual counties. When this is done, we see that the average lead time to the first tornado in each county in a tornado watch is 3.3 hours and the average lead time to the first severe thunderstorm report in each county is 3 hours. While the ideal would be for every tornado to be in a tornado watch, the state of the science makes it a realistic goal to have all occurrences of 3 or more tornadoes within an area of 25,000 mi^2 of any intensity or of any strong or violent tornado (F2-F5) in a tornado watch.

These materials demonstrate that addressing the severe weather threat in the United States is a difficult task, and anything that would make the job easier certainly would be welcome. The Early Alert Method for severe convective weather was proposed and developed under SBIR 2 with this in mind, and plans were being made for real-time tests of the methodology during the tornado season of 2008. Before this could be done, however, the method had to be automated for real time application. How this was done is addressed in the next section of this report.

5.0 AUTOMATING THE EARLY ALERT METHODOLOGY

Considerable progress had been made on the SBIR-2 calls for automation of the severe storm detection algorithm during the first year of the SBIR-2 effort. During the work it was noted that the imagery from GOES-12 is inferior for project purposes to that from GOES-10 and GOES-11, because the 12 μm infrared channel had been replaced by a single CO_2 channel. Thus, a way had to be found to replace the 12 micron infrared channel with the CO_2 channel by developing a method to mask the broken and thin clouds. Of most consequence was the automation of the Rosenfeld analysis methodology and its incorporation into the overall system. This was a major milestone. Quantification of the severe weather threat was done by

calculating Early Alert scores using the scoring scheme presented Table 2. The focus was then on improving and testing the overall system.

The full story of how the Rosenfeld Early Alert Methodology was automated and tested is told in Appendix A of Woodley et al. (2008) by Guy Kelman, who did most of the work. It is provided there for documentation purposes and for scientific posterity.

Table 2 Procedure for the Calculation of Severe Storm Scores by Satellite Image

(Now done in the Automated Algorithm)

For the satellite field of view the following parameters are calculated for each pixel of 4x4 km:

1. Determine cloud top temperature (T).
2. Visible reflectance is corrected for the solar zenith angle.
3. Statistics of the HRV (mean, variances, skewness)
4. Texture roughness parameters (based on the HRV channel)
5. Apply the cloud mask.
6. Calculate cloud-top-particle effective radius (Re).

The whole satellite field is scanned sequentially with windows of 26x26 4-km pixels. Thus, each score window is roughly 100 km on a side. The window is advanced at steps of half of a window (13 pixels), both east-west and north-south. The window size is a parameter that can accept any even value.

For each window the T-Re relations are calculated as follows:

1. For each 1°C temperature interval a Re value is assigned. For each 1°C temperature interval there are three possibilities:
    a. There is no cloudy pixel that has that T. The Re for that T remains missing.
    b. There is one cloudy pixel with that T. The Re is taken from this same cloudy pixel.
    c. There is more than 1 cloudy pixel. The Re values are sorted and, for example, the 30^{th} percentile of the Re might be matched with that T. The percentile value (30) is a parameter that can be set as any number between 0 and 100.
2. The T-Re function undergoes running averaging, where Re of each T value is averaged with its immediate neighbors in the T dimension, weighted by the number of pixels that contribute to each T 1°C interval.
3. Further averaging with its immediate neighbors points which are local maxima in values of Re. If Re of the immediate neighbor is missing, average with the next one instead, if not missing too.

For each calculation window the set of computed T-Re relations are used to determine the "severe storm score" for that window. The score is a multiplication of several parameters having values between 0 and 1. The larger the score the greater the probability there is of a severe storm. If a parameter is 0, it means that it alone can disqualify the window from being a candidate for a severe storm. A value of 1 means maximum probability based on this parameter alone, but it might be overridden by multiplication with another parameter with a 0 value. The overall score is the n^{th} root of the multiplication of the n values of

the individual parameters, multiplied by 1000.

The scores of individual parameters are computed as follows:

1. Tb, cloud base temperature. Tb is T of the warmest cloudy element in the T-Re table. For reducing distortion due to ground effects, the warmest T is rejected if it has a Re greater than the Re of its neighbor colder element and the number of pixels composing it is smaller than the number of pixels composing the neighboring element. Then Tb is replaced with the colder neighboring T. This test is also applied on the new Tb and so on until it is no longer satisfied. The score is calculated as Tb/10. If the result is <0, then Tb=0; If the result is >0, then Tb=1.
2. Ttop, the coldest cloudy T in the window.
   Ttop_score=-(Ttop-(-38))/12.

   if(Ttop_score<0)Ttop_score=0

   if(Ttop_score>1)Ttop_score=1
3. ReGlac, the Re at the glaciation temperature.
   ReGlac_score=(43-ReGlac)/20.
4. Tg, glaciation temperature. Tg must be between -1 and -40°C. If Tg is warmer than -40°C it is assigned as the warmest T that had reached the largest values of Re in the T-Re profile.

   Tg must be smaller than To as depicted by the ReGlac-To relations in Figure 10.

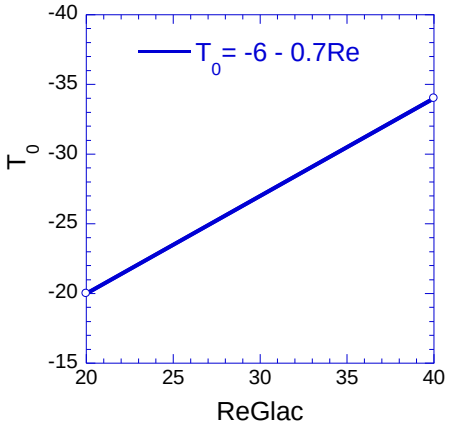

Figure 10: The maximum allowed Tg for a given ReGlac.

   The Tg_score=(To-Tg)/(To+40) If the score is <0, then the score is 0

5. Gapmax, Length of largest gap of missing data in the T-Re table, in °C. Gap_score=1-Gapmax/10
6. Corm40s, the correlation between T and Re in the smoothed T-Re table, for the section between Tb and -40°C.
   Corm40s_score=5*(-0.8-Corm40s)
7. T14 is the temperature at which Re reaches 14 μm. Tlinmin is the T of the top (coldest T) of the linear part of the T-Re relation. The slope is defined as -dRe/dT, i.e., the increasing rate of Re with decreasing T [μm $°C^{-1}$].
   If(T14<Tlinmin)
   SlopeChange=SlopeT14Tg-SlopeT14Tb, where Slope14Tg is the slope between Tg and T14, and SlopeT14Tb is the slope between T14 and Tb.

   If(T14>Tlinmin)
   SlopeChange=SlopeLG-SlopeTL,

where SlopeLG is the slope between Tg and Tlinmin, and SlopeTL is the slope between Tlinmin and Tb.

SlopeChange_score=(0.6-SlopeChange)/0.6

8. Slopemin is the minimum slope between Tb-5 and T=-40°C. Slopemin_score equals 1 except for the case that Slopemin<0 and T at the point of Slopemin is at least 10°C colder than Tb. In such a case Slopemin is set to 0.

These complex procedures were applied initially on an exploratory basis to the GOES-10, and then also to GOES-12. An interactive process of fitting the parameters was based on testing cases where the prediction failed, making a fix and testing it again on past cases to see that it did perform on them at least as well as the previous version.

At this point the technical difficulties of assessing severe storm potential over an area of interest using archival data had been overcome. It was time to test the methodology in real time. And it was imperative to understand the nature of the real-time data flow. In this respect assistance with access to the real-time data was needed from NOAA, which is directly in charge of the SBIR 2 project. It was time to brief NOAA personnel on the progress of our SBIR 2 efforts and to make contact with the NOAA person who would enable us to establish a link to the real-time data provider within NOAA. In addition, we needed to link our method with potential sounding predictors of tornado activity such as wind shear, CAPE and storm-relative helicity in order to develop a method that considers all factors. This definitely would require coordination with NOAA people.

SBIR-2 calls for automation of a severe storm detection algorithm and its running on GOES-10 and GOES-12 satellite imagery. Progress had been made in reaching this objective during 2007. In October 2007 after completion of the second quarter, our group traveled to the offices of the Storm Prediction Center in Norman, OK to demonstrate the capabilities of our developed system to detect regions of imminent severe storm potential based solely on the analysis of GOES multi-spectral satellite imagery.

This capability depends on the NOAA geostationary meteorological satellites providing the needed temporal and spatial coverage for the continental United States. The demonstration was performed on selected known past cases, indicating that our automated procedure has potential for improved watches and warnings for severe storms with lead times of up to 90 minutes. This capability provides an improvement to state of the art numerical weather forecast programs in the time window where the numerical forecasts suffer from spin-up numerical instability. Therefore it was greatly appreciated by the members of the SPC, both the management and the field officers who attended a lecture delivered by Prof. Rosenfeld. Based on the meetings in October 2007, it was decided to set up an experiment on location with real-time satellite and forecast feeds. The start date of the experiment was set for early April 2008. These tests were done under the name "The Early Alert" Project (EAP).

6.0 THE REAL-TIME TESTS OF THE METHODOLOGY IN OKLAHOMA

6.1 Preparations and Operations

The field test of the Early Alert Project (EAP) began with the arrival of Guy Kelman in Norman, Oklahoma on April 9, 2008. Guy began by using the CIMMS

office (Room 3221) to connect with the flow of GOES 11 and GOES 12 imagery and the RUC data that was set up for us by Bob Rabin of NSSL. How this was done is explained by Guy Kelman in some detail in Appendix A of Woodley et al. (2008).

The satellite data were fed into a laptop that was nick-named GIZMO and then it was split off to a MAXTOR hard drive where the data were archived and to another notebook computer nick-named ELWOOD where the data could be manipulated and monitored. This is where the real-time data could be displayed for Early Alerts on a large monitor and then converted manually to PNG files by hitting the "snapshot" button on the computer monitor. This PNG snapshot archive for the day remained on the computer until the evening when it was removed in preparation for the next day. To obtain the PNG files for previous days it was necessary to retrieve them from the archive using a special procedure.

It took several days to get the system up and operating. Dr. Rosenfeld joined Guy Kelman in Norman on April 13th and then left on April 20th for the joint AMS/WMA meetings in Westminster, Colorado. On April 25th Dr. Rosenfeld and his wife Malka left the Woodley home in Colorado to return to Israel. Dr. Woodley then traveled by air to Norman, Oklahoma on April 28th, arriving mid-day. He rented a car and drove to the Residence Inn in Norman, where he registered for an extended stay. Dr. Woodley then went to the National Weather Center off HWY 9 on Jenkins Street to join Guy Kelman, where the EAP effort had been provided office space.

It took a while for Dr. Woodley to get familiar with the system that Mr. Kelman had devised and implemented. It involved pulling the processed images onto the monitor screen as they became available. These were then snap-shotted into the system to create a PNG file and then they were examined for the existence of Early Alert boxes. When he hit the snap-shot button on a given file it was posted on the EAP website at (http://severe-storms.net). It was intended that ultimately the forecaster would go to this site to see the latest Early Alert from the methodology. The problem was that the score numbers within the Early Alert boxes were illegible even on the mapped product. This needed work. If Dr. Woodley forgot to hit the snap-shot button no PNG file was created and it would have to be created later from the archive. An example of the thousands of images generated during the real-time tests of the methodology is provided in Figure 11 for a processed image from GOES-11 at 2030 UTC on April 23, 2008. The Early Alert boxes are superimposed on the image. The severe storm scores are shown within the boxes.

Before Guy Kelman and his family (wife and 4 children) left Oklahoma on the afternoon of May 2, 2008, Dr. Rosenfeld had discovered a minor error in his methodology that he eliminated over the course of a couple of days. After this problem was eliminated the old cases had to be rerun. After they had been rerun they had to be interfaced with a new program written by Guy that permitted the comparison of the locations of severe weather as documented by the Storm Prediction Center with the Early Alert boxes generated by the Rosenfeld satellite methodology. In the versions shown by Guy to Dr. Woodley a map showing the position and type of severe storm reports over the past half-hour or hour was shown. Then he went back 2 hours prior to the ending time of the storm plot and progressively showed the EA boxes on the map. In stepping through the sequence many times it was possible to determine at least qualitatively whether there was a

relationship between the EA boxes and the plotted storm points.

An operational summary of the Early Alert field tests is provided in the tables of Appendix B in Woodley et al. (2008).

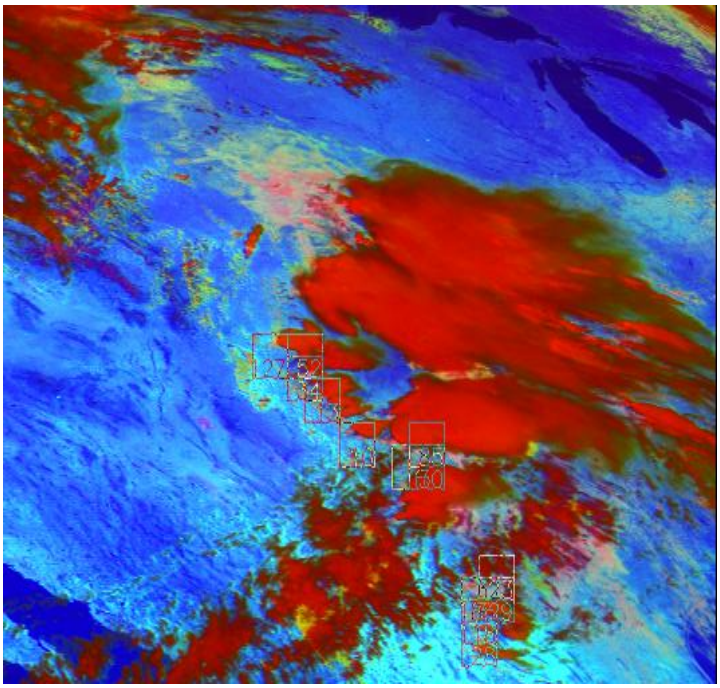

Figure 11. GOES-11 multi-spectral satellite image at 2030 UTC on April 23, 2008. The image has been colorized according to the method of Rosenfeld as described in the caption for Figure 1. Each box superimposed on the image represents an Early Alert. The number within the box is the severe storm score. Comparable images were generated for the daylight hours with adequate solar illumination during the Early Alert Project.

6.2 Analysis Procedures

In doing the analyses it was important to address the question whether the new satellite methodology could provide verifiable Early Alerts of imminent severe weather that would assist SPC with its mission to protect lives and property.

The input data for the analyses of method effectiveness included the following:

- The Early Alerts (EA) obtained upon applying the method to individual GOES-11 and GOES-12 images on all days between 23 April and 5 June (inclusive) 2008. This included the dates, times, positions (lat/long) and scores of all EAs. Each EA was a box 100 km on a side, so its position was the center of the box.

- The reports of severe weather compiled by the Storm Prediction Center (SPC) for each day in the period of interest. This included the type of severe weather (i.e., tornado, hail and strong straight-line winds), its intensity and the time and location (lat/long) of its occurrence.

- Documentation of weather watches (Severe Thunderstorm and Tornado) issued by the SPC. This included the time period (start and end) of each watch. The location of each watch was quantified by recording the positions of the vertices of a polygon (usually a quadrilateral) that encompassed the counties within a state or states that were subject to the watch.

- The Severe Weather Warnings issued by local WSFOs based on real-time radar data and/or reports from the general public. The positions of the severe weather warnings, which are limited normally to relatively small areas, were obtained by recording the center point of the warned area.

Thus, two of the four sets of data were anticipatory of severe weather (i.e., EAs and Weather Watches) and two addressed severe weather that had

already taken place (i.e., severe weather reports and severe weather warnings that were compiled at the end of the day).

It is helpful to recount the events of a typical day to facilitate understanding of the EA methodology, how it works and how the EA estimates are related to the severe-weather reports and watches and warnings. The method requires adequate solar illumination for derivation of the T-re profiles that are input to the calculation of the EAs. The GOES-11 and GOES-12 satellites viewed in 15-min intervals the west-central and east-central portions of the United States, respectively, during the period of study. (The ability to use GOES-11 imagery to look at remote areas of the Mountain West where radar coverage can be unreliable should prove valuable to the SPC and the National Weather Service for short-term forecasting of imminent severe weather.) There was some overlap in coverage over the central United States. Adequate light for GOES-12 EA calculations was present in the period from roughly 1300 to 2230 UTC. The time period for GOES-11 was from roughly 1500 UTC to no later than 2330 UTC. In the absence of synoptic forcing the two GOES satellites normally covered the onset of the convective cycle, but there were many instances when strong convection continued into the twilight and night hours, making EA calculations impossible.

Evaluating method performance was a major challenge. The focal point of the evaluation was the EA values generated by both satellites. During the analysis phase the time, position, score and movement of the area first delineated by each EA was recorded and it was compared to the severe-weather reports, severe weather warning issued by the local WSFO's, and the watch areas issued by the Storm Prediction Center (SPC). This comparison was done for up to 3 hours forward in time from first identification of an EA for match or search radii of 0^o, 0.5^o, 1^o, 1.5^o and 2^o around the position of each EA. Allowance was made for the downwind movement of each EA during the matching process such that the downwind boundary of the search area around an EA moved downwind with the speed and direction of the pressure weighted mean wind in the layer 0 to 6 km (i.e., the pressure-weighted mean winds from 0 to 6 km in a single layer of RUC data). If the position of a storm report or severe weather warning fell within these radii around the EA within the 3-hr period, it was a Hit. Those occasions when the EA was not verified by a report and/or warning were called "False Alarms." This forward matching process is illustrated in Figure 12.

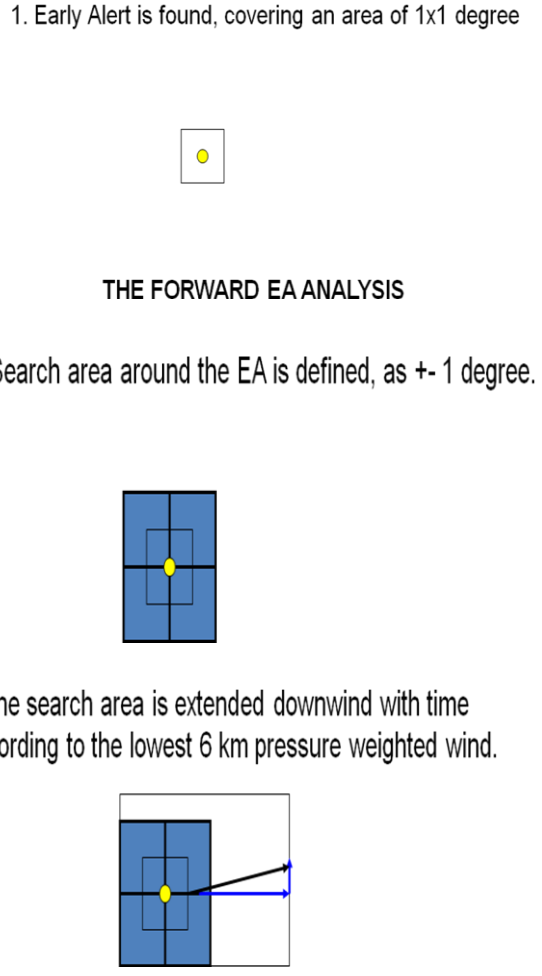

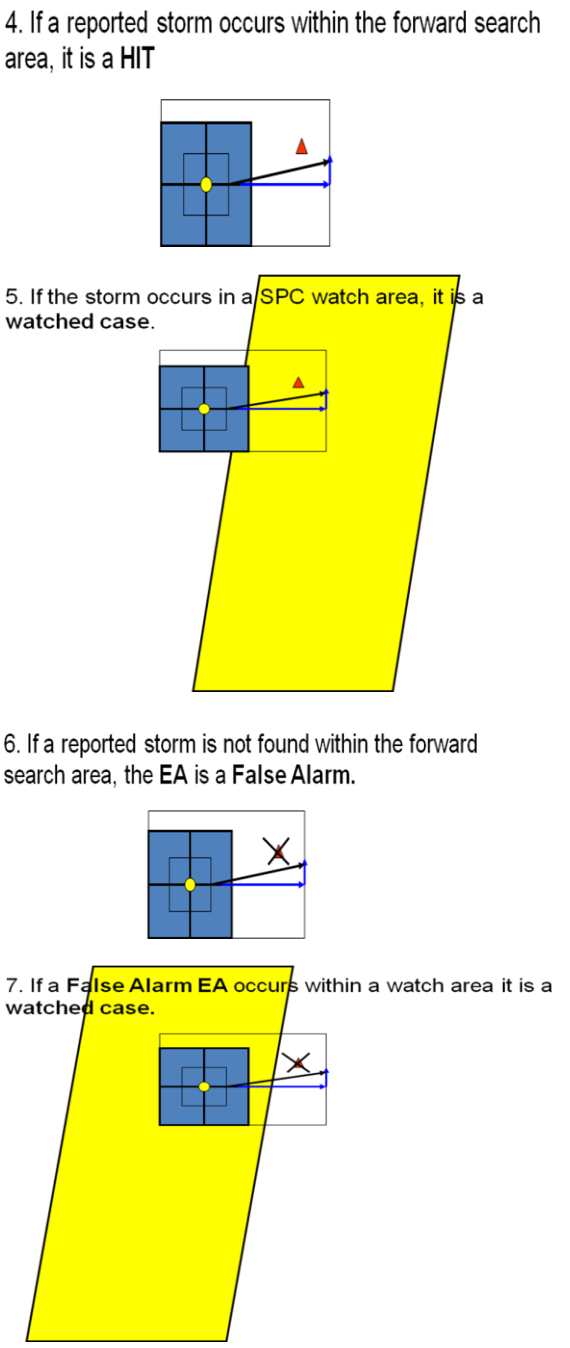

Figure 12. Schematic illustration of the EA forward matching process.

In this forward matching process the EA can fall into three possible categories: 1) false alarm, 2) storms already in progress and 3) EAs that will be verified as hits in the future, where False Alarms are not verified by a future report or warning within the search area, storms already in progress are those that exist at the time of the EA and hits are those that are verified by storm reports or warnings in the future. Thus, the False Alarm rate is the ratio of the false alarm sample to the entire three-category sample. Calculation of the false alarm rate by including the continuing storms in the calculation minimizes the estimate of the false alarm rate. Some would argue that "taking credit" for the continuing storms in all calculations of method performance is inappropriate and that they should be deleted. This was done in our assessments.

Similarly, each actual severe weather occurrence, as indicated by Reports or Warnings, was searched backward in time using the same search radii for preceding EAs that had potentially predicted it. This process is illustrated in Figure 13. In this backward analysis the storms in progress or continuing storms were deleted as was the case with the forward matching analysis. They were not included in the matching analysis. When a verifying report or warning was predicted by an EA, it was called a "Hit." When the verified report had no preceding EA within its backward search area it was called a "Miss". The backward analysis was the only way that the "Miss" rate could be determined for all storms and warnings. The lead time for a particular storm (i.e., report and/or warning) was the time between the time of each storm and the corresponding first EA of that storm (See Figure 14). Inclusion of all EAs for a particular storm before the reported or warned occurrence of the storm would underestimate the averages of the actual lead times.

1. A Severe Storm Report or WFO warning is found.

THE BACKWARD EA ANALYSIS

2. Search area around the Storm is defined, as +- 1 degree.

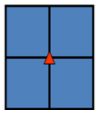

3. The search area is extended upwind backward with time according to the lowest 6 km pressure weighted wind.

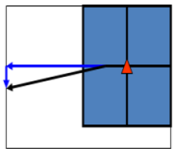

4. If an Early Alert, whose location is defined by its central coordinates, occurs within the backward search area, it is a **HIT**.

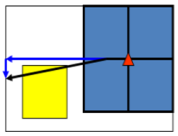

5. If the storm, defined by a report or warning, occurs in a SPC watch area, it is a **watched case**.

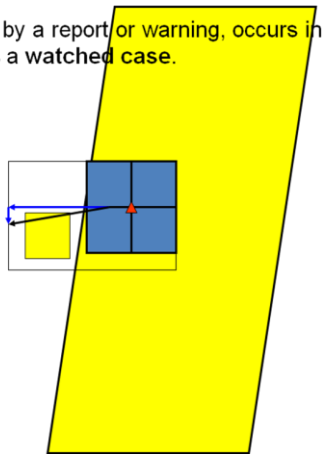

6. If an Early Alert does not occur within the backward search area, it is a **MISS**

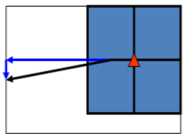

7. If a storm which is **MISS**ed by the EAs occurs in a SPC watch area, it is still a **watched case**.

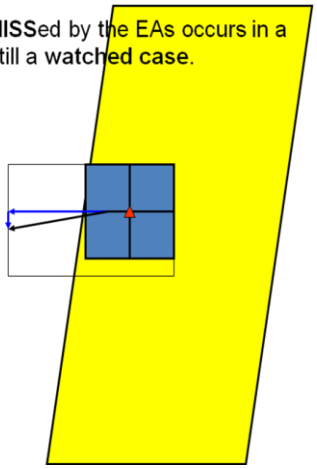

Figure 13. Schematic illustration of the EA backward matching process.

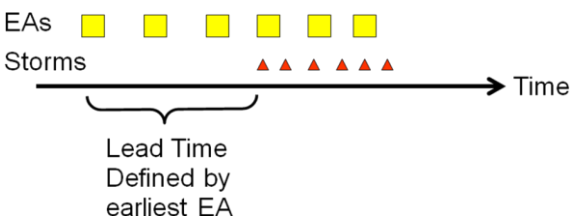

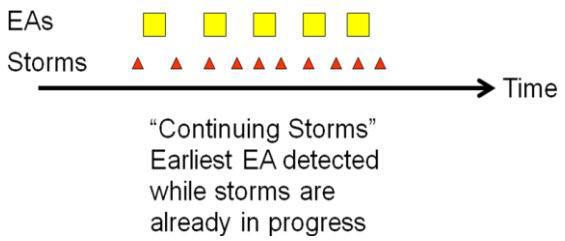

Figure 14. Illustration of the calculation of EA lead times (top) and what is meant by "Continuing Storms" (bottom).

During the forward and backward analyses, it was determined whether the EA, report or warning fell within any SPC watch areas (See Figures 12 and 13). When any of the reports or warnings fell within a SPC watch area, they were called "Watch Cases" for their comparison with EA values. When the reports or warnings fell outside a watch area, the cases were called "Non-Watch" cases for their comparison with the EA values. There were a significant number of instances of report-verified and/or warning-verified EAs without corresponding watch areas. These cases could be considered SPC misses because the severe weather occurred outside the boundaries of watch areas.

The evaluation was done for G-11 and G-12 imagery separately and for G-11 and G-12 combined for the following areas:

- Tornado Alley: from 27^{o}N to 40^{o}N and 90^{o}W to 103^{o}W;
- Central & Eastern USA: from 27^{o}N to 45^{o}N and 70^{o}W to 105^{o}W;
- No bounds. All satellite viewing area over North America and the adjacent seas.

The imagery from the G-11 and G-12 satellites overlapped primarily in the tornado alley region.

Although there is no one single best analysis, the first analysis swath that inputs the data from both satellites is preferred. Three hours were allowed for the matching of each EA. With respect to spatial matching of EA values with reports and/or warnings a search area of 1^{o} around each EA point is the preferred one. Even so, everything was examined and compared: the EA method performance for G-11 and G-12 imagery, the results for watch and non-watch areas for variable search areas, the results as a function of EA score and the lead times between an EA value and the subsequent severe weather.

6.3 Results of Analyses

Although a large amount of information was generated during the analysis, the analysis permutations thought to be most meaningful are presented here. The results thought to be most representative of method performance was for the "Tornado Alley" region viewed jointly by the G-11 and G-12 satellites. Although the method performed slightly better for G-11 than G-12 imagery, both were included in this analysis to maximize the sample size. This dichotomy was not a surprise since, as discussed earlier; a major pre-test effort was made to compensate for the missing 12 μm infrared channel on this satellite.

The forward and backward EA analyses for a 3 hr match time and a 1^{o} match area, partitioned by watch status (i.e., no watches, watches and all) with continuing storms excluded are given in Table 3. The initial focus is on the left half of the table in which the results of the forward matching analyses are presented. Beginning with the "No Watch" partition, note that there were 504 EAs for which there was a false alarm rate of 60.3% and a hit rate of 39.7%, or 200 out of the total sample of 504. This number is highlighted in red below the overall sample of 504 in this partition. The average lead time is slightly over an hour at 69.7 minutes. The hit rate for the SPC is 0% because none

of the 200 verified EAs occurred in a watch area.

There were 159 EAs in the Watch partition. Of these, the False Alarm rate was only 22% as compared to 60.3% for the No Watch partition. This better method performance is likely due to the expertise of the SPC forecasters who identified the watch area as primed for severe weather activity. Fewer false alarms would be expected for such primed areas. For the same reason, the hit rate for the EAs in the watch areas is higher too (i.e., 78% vs. 39.7%). The average lead time between the EA and the subsequent severe weather is 71.5 minutes for this category. There were 124 verified EAs in the watched areas, so the SPC would have to be credited with hitting all (100%) of these by their watches.

The combined category of Watches and Non Watches has an overall sample of 663 EAs of which 324 were verified by storm reports or warnings. The overall EA false alarm rate is 51.1 % and the EA hit rate is 48.9%. The SPC watch percentage hit rate is 38.3% (i.e., 124/324 = 0.383) with respect to its watch areas. The average lead time is 70.4 minutes.

The second focus is on the right half of Table 3 that gives the results of the backward analyses of the storm reports and warnings. The results in red pertain to the backward analyses of the SPC storm reports. Again, the results are partitioned as a function of watch status. There were 917 reports of severe weather that did not fall into a SPC watch area. The hit and miss rates for the EAs in this category are 49.1% and 50.9%, respectively The SPC hit rate for these storm reports is 0, because none of them occupied any of their SPC watch areas. The mean lead time is 116.8 minutes.

There were 686 reports of severe weather that fell into a SPC watch area. The hit and miss rates for the EAs in this category are 63.3% and 36.7%, respectively. Again, method performance is better for the watch areas because of the identification by SPC of a higher threat of severe weather for the watch areas. The mean lead time is 91.4 minutes. The mean lead time is 91.4 minutes. The SPC hit rate for these storm reports is 100%, because all of them initially were in one of the SPC watch areas.

The overall sample is 1603 severe weather reports. The overall hit and miss rate are 55.1% and 44.9%, respectively. The comparable figures for SPC with respect to its watch areas are 42.9% and 57.2%, respectively. The avg. lead time is 99.8 min.

The results for the comparable backward analysis for the severe storm warnings are presented in blue in the right half of Table 3. Note the EA method performed a few percentage points better across the board than the analysis with respect to the severe storm reports. The SPC performance relative to its watch areas is slightly better too. The improvement is less than 10% in all cases. The overall mean lead time for the backward severe-storm warning analysis is 124.1 minutes.

Table 3: Results of SBIR-2 Analyses

Forward Analysis of Early Alerts (Continuing Storms Excluded)					Backward Analysis from Storm Reports and WFO Warnings (Continuing storms excluded)			
Watch Class	N EA	% Hit (%False) EA	% Hit SPC	Avg. Lead Time (minutes)	N RPTS WARNS	% Hit (%Miss)	% Hit (%Miss) SPC	Avg. Lead Time (minutes)
No Watches	504 200	39.7 (60.3)	0	69.7	917 361	49.1 55.4 (50.9) (44.6)	0 0	116.8 126.0
Watches	159 124	78.0 (22.0)	100	71.5	686 454	63.3 66.5 (36.7) (33.3)	100 100	91.4 122.6
All	663 324	48.9 (51.1)	38.3	70.4	1603 815	55.1 61.6 (44.9) (38.4)	42.8 55.7 (57.2) (44.3)	99.8 124.1

6.4 The Relationship between Verified Early Alerts and the SPC Watch Areas

This research effort was promoted with the expectation that it would assist SPC with its severe weather forecast and watch responsibilities through the early identification (Early Alerts) of cloud groups and cloud systems that are about to produce severe weather. The results presented above indicate that the Early Alert method developed during the course of the research has been successful in flagging severe weather events an average of two hours before they occur. The percentage of severe-weather false alarms has decreased and the frequency of severe-weather hits has increased with the new methodology relative to what was possible by SPC for the same sample. This was the primary goal of SBIR-2 at the outset.

A closer look at this issue is possible by plotting on a daily basis the locations of the Early Alerts, which have been verified by either severe weather reports and/or by severe weather warnings, relative to the

plots of the watch areas on the same day. An example of the plots is given in Figure 16 for May 10, 2008, the same day addressed in Figures 8 and 9.

There is a lot of information in Figure 16, so it is worth taking some time to understand this figure. Comparable plots for all days of the project are given in Appendix D of Woodley et al. (2008). Each rectangular box is a **verified** (by report and/or warning) EA. The color coding gives the time of the EA by relating its color to the time color code at the top of the figure, which covers the period that EA calculations were made from 1400 to 2345 UTC. Thus,

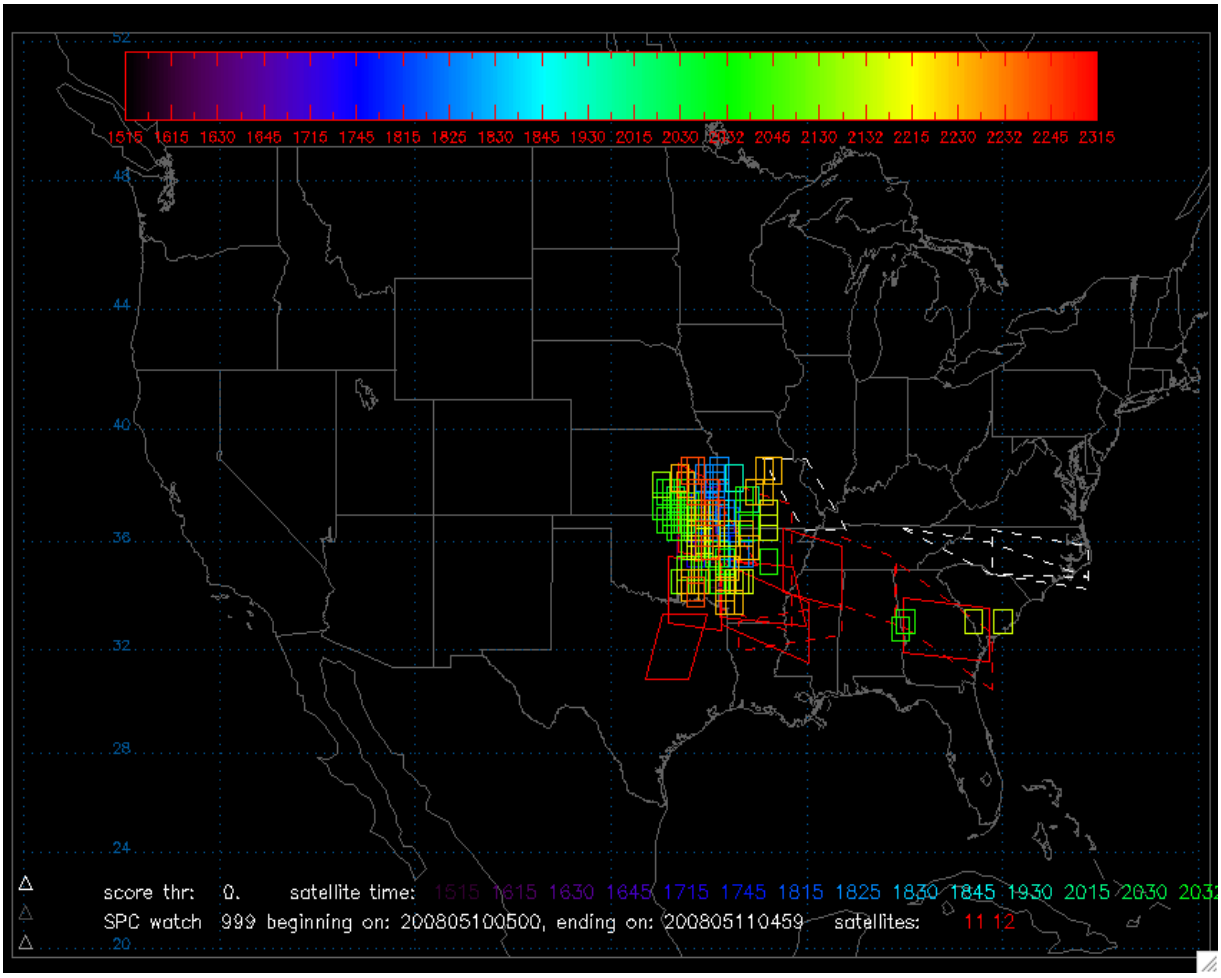

Figure 16. Plot of report- or warning-verified alerts (EA) (color-coded small boxes) on a map of SPC watches (red for tornado and white for severe thunderstorm) for May 10, 2008. Solid watch boundaries were valid during the period of EA estimation whereas the dashed watch boundaries were valid outside the period of possible EA estimation.

the EA boxes are green and yellow after 2030 UTC but before about 2230 UTC and they are orange thereafter. No EA estimates were made after 2345 UTC. The plotted polygons are all of the SPC watches for the day. If the sides of a plotted polygon are solid, it means that the watch was valid during the period that EA estimates were made. If the sides of the polygon are dashed, it means that the watch was valid outside the period of EA operation and no EA comparisons should be made. If the plotted watch is white it is a severe thunderstorm watch; if it is red, it is a tornado watch.

The purpose of this presentation is to gain overall impressions of the relationship of the verified EA values to the SPC watches to see whether the EA program might have been helpful to SPC on this day. There is no intent here to attempt here to evaluate SPC performance. If that were to be done, it would have to involve plots of individual watch polygons on which the locations of verified EAs, the locations of storm reports and warnings have been superimposed. That would involve a major additional effort.

The overall impression from Figure 16 is that the storm-verified EA values and watches agreed very well for the areas (southeast Kansas, northeast Oklahoma and western Arkansas) that had tornadoes and resulting fatalities. In fact, there are so many EA values in these regions that it is impossible to see the SPC watch areas underneath the plotted EA values. There were, however, a number of tornado watches during the EA period of calculation that had no verified EA values such as those in northeast Texas, eastern Arkansas, and western Kentucky and Tennessee. There is nice agreement between the EAs and the watch in Georgia. Nothing can be said about the dashed watch polygons because no EA calculations could be made for the watch period because of poor or non-existent solar illumination.

Note there were EAs with verifying severe storms in northeast Florida on this day without any corresponding watch areas. It is obvious from the plots that the primary region of concern on this day was in the central United States with Florida probably of lesser concern. Here is where the EA methodology might have helped. If the credibility of the method had been established and if it was one of the tools used routinely at SPC, their forecaster might have considered issuing a watch on this day for northeast Florida.

Examination of the rest of the plots provided in Appendix A of Woodley et al. (2008) was an interesting exercise. There were many cases when it appeared that the EA methodology would have been helpful to the SPC forecasters by drawing their attention to threat areas outside the major regions of current interest. A summary of the comparisons is given in Woodley et al., 2008).

7.0 DISCUSSION

A number of problems and challenges were encountered during the tests of the methodology. Automating the methodology, writing the software, accessing the needed data, configuring the system and getting it operative were major challenges in the time-frame that was set for the accomplishment (by mid-April 2008) of these tasks. A few problems were encountered during the tests. For a given satellite, the EA estimates were not always stable from one image to the next such that EA estimates at one time had disappeared in the next only to reappear in a later image. Although such variability may merely be indicative of natural changes in the clouds, it happened often enough to raise some concerns about the stability of the imagery and/or the methodology. When it

occurred, it decreased the real-time confidence in the EA product, thereby compromising the interactions with the SPC forecasters (See section 6.4 by Golden). This variability is yet to be explained. It is suspected that angular fluctuations in the phase function of the ice crystals that are not taken into account by the effective radius retrieving method are responsible.

The original work plan for the Oklahoma tests called for posting EA maps on a website for real-time retrieval by the SPC forecasts. This plan was never implemented satisfactorily because the EA scores on the posted EA maps were illegible. Further, the forecasters had not been briefed adequately about the test program. Only when Dr. Golden became involved did meaningful interactions take place. On many occasions he hand-delivered legible EA maps to the duty forecasters and interpreted the maps with them. The interactions were polite and courteous, but it is unlikely that anyone had been convinced of the value of the EA maps before the test program ended on the evening of June 5, 2008. Funds permitting, the method tests should have run the entire spring and summer season.

The EA methodology was never tested under the conditions for which it is ideally suited by alerting in advance isolated, surprise storms that occur during the long summer and fall seasons, outside the typical spring and early-summer severe-weather season. Even though a forecaster may figuratively "be asleep at the switch" late in the season when his/her guidance does not suggest much possibility of severe weather, the new satellite-based method operates continuously and tirelessly by scanning the entire satellite view area for clouds that show imminent severe-weather potential. Even during the prime severe weather season the daily plots of verified early alerts identified several occasions when a severe weather watch would have been warranted. The potential exists, therefore, for potentially saving lives and protecting property through systematic long-term application of the early alert methodology, when it is combined with the expertise of the SPC forecasters.

8.0 CONCLUSIONS

The method to provide verified Early Alerts (EA) of impending severe weather has been developed and tested successfully in a real-time environment. This was the goal of the SBIR-2 research effort under Woodley Weather Consultants from its outset. The methodology actually works better than was envisioned by Dr. Woodley when it was first promoted for funding to the NOAA SBIR Program office. Within the central United States, which has been nicknamed "Tornado Alley", where there is overlapping coverage of the GOES-11 and GOES-12 satellites, the EA false alarm (FA) rate during the real-time tests using a match area of 1^{o} averaged 25% overall, greater for non-watch cases and less for watch cases. The Early Alerts were verified by severe weather warnings and reports at a rate of about 70% to 80%, respectively. Thus, the method appears to work equally well regardless of the method of validation (i.e., reports or warnings). It was noted that the FA rate decreases as the EA score increases, but percentage "Hit" or validation rate decreases. Thus, there is a tradeoff between the FA rate and the Hit rate. The lead times between the Early Alerts and the occurrence of the severe weather events averaged close to two hours. This provides compelling evidence for the utility of the EA methodology for improving severe thunderstorm and tornado warnings from local forecast offices. Method performance degraded slightly for larger viewing areas, for larger match areas and for imagery from the GOES-12 satellite that lacked the crucial

12 μm infrared channel. Even so, the results of method application are highly consistent, no matter the viewing and match areas and the method of EA validation.

9.0 RECOMMENDATIONS

In its first real-time test the new satellite-based method to provide Early Alerts for impending severe convective storms (tornadoes and hail) has been shown to work exceptionally well such that prolonged use in an operational context may save lives and property. The primary recommendation, therefore, is that the method be developed and tested further so that it can reach its full potential. Within the context of this primary recommendation the following additional recommendations are made:

- The full analysis should be repeated with the exclusion of the continuing storms.
- Real-time tests of the methodology should be continued for the entire 2009 season (April through September) in conjunction with the Storm Prediction Center (SPC) and the VORTEX-2 field campaign. Because funding for the continuing tests can no longer come from NOAA's SBIR program office, new NOAA funding will have to be sought from SPC itself and/or from NOAA's National Environmental Satellite Data & Information Service (NESDIS).
- The Early Alert (EA) methodology should be integrated into the daily operations of the SPC during the 2009 real-time tests.
- Problems and uncertainties should be investigated during the additional recommended tests, including the image-to-image stability of the EA estimates,
- The older NOAA GOES satellites with the 12μm channel should be used in preference to the newer GOES satellites without this crucial channel. These results should be used by NOAA and its partners in NPOESS and especially GOES-NEXT to ensure retention of high-quality multispectral imaging capability in future satellites, with rapid data access.

The second major recommendation is that the Early Alert methodology should be marketed to potential users. This is the primary purpose of the Small Business Innovative Research (SBIR) research program. Although the marketing should be done under the umbrella of Woodley Weather Consultants (WWC), members of the current research team (Woodley, Rosenfeld, Golden and Kelman) likely will be involved in the marketing and share in its profits. In pursuing a marketing plan it is recommended that the following be considered:

- A decision must be made whether WWC or an adjunct entity will generate the EA estimates internally and provide the results to potential users or whether the methodology will be sold to potential users for their internal use. Selection of the second option will require a high level of technological sophistication by the user and training by WWC personnel in the use of the method. It is envisioned that the marketing will require a mix of these two options.
- A list of potential users/buyers of the methodology should be developed as an integral part of the marketing

plan. Foremost among them should be the SPC whose operations should be improved considerably through the use of the new methodology. An outright purchase of the method and training in its use should be pursued by the SPC or another NOAA entity. In addition to NOAA, the method should be marketed to: 1) highly weather-conscious, competitive television stations, especially the Weather Channel, 2) organizations such as Weather Decision Technology (WDT) in Norman, Oklahoma that provide a range of weather-data services to clients, 3) individuals and organizations outside the United States that are involved with warning of severe storms, and 4) groups that are involved in hail suppression projects around the world

ACKNOWLEDGEMENTS

The authors gratefully acknowledge the assistance provided by several groups and individuals to Woodley Weather Consultants (WWC) under its SBIR II NOAA grant to provide early alerts (time and locations) of impending severe convective weather (i.e., tornadoes and large hail). In addition to the Storm Prediction Center (SPC) under the direction of Dr. Joseph Schaefer, we were provided help from NSSL, CIMMS and the University of Oklahoma. Russ Schneider, David Imy, and Steve Weiss of SPC were very helpful. Others at SPC who helped us were Peggy Stogsdil, John Hart, Phillip Bothwell, Jay Liang and Joe Byerly.

Others who helped us were Kevin Kelleher Deputy Director at NSSL and Jeff Horn of NSSL and Peter Lamb and Tracy Reinke at CIMMS who worked with Russ Schneider. Incredibly helpful to us throughout was Bob Rabin of NSSL, who provided us access to the needed GOES 11 and GOES 12 multispectral satellite data through SSEC and NESDIS-DC for the project.

Finally, we express our satisfaction and gratitude with NOAA's SBIR program. We are happy to have had the opportunity to compete for and win the SBIR II award.

REFERENCES

Adler R.F., M.J. Markus, D.D. Fenn, 1983: Detection of severe Midwest thunderstorms using geosynchronous satellite data. *Mon. Wea. Rev.*, **113**, 769-781.

Andreae M. O., D. Rosenfeld, P. Artaxo, A. A. Costa, G. P. Frank, K. M. Longo, and M. A. F. Silva-Dias, 2004: Smoking rain clouds over the Amazon. *Science*, **303**, 1337-1342.

Arking, A., and J. D. Childs, Jeffrey D., 1985: Retrieval of cloud cover parameters from multispectral satellite images. Journal of Climate and Applied Meteorology, Boston, **24**(4): 322-333.

Beard K. V. and H. T. Ochs III, 1993: Warm-Rain Initiation: An Overview of Microphysical Mechanisms. *Journal of Applied Meteorology*, 32, 608–625.

Brooks H.E., J.W. Lee, J.P. Craven, 2003: The spatial distribution of severe thunderstorm and tornado environments from global reanalysis data. *Atmospheric Research* **67– 68**, 73– 94.

Brooks, H. E., and R. B. Wilhelmson, 1990: The effect of low-level hodograph curvature on supercell structure. Preprints, 16th Conf. on Severe Local Storms, Kananaskis Park, AB, Canada, Amer. Meteor. Soc., 34–39.

Browning K.A., 1964: Airflow and precipitation trajectories within severe local storms which travel to the right of the winds. *J. Atmos. Sci*., **21**, 634-639.

Browning K.A., R.J. Donaldson Jr., 1963: Airflow and structure of a tornadic storm. *J. Atmos. Sci*., **20**, 533-545.

Davis J.M., 2006: Tornadoes in environments with small helicity and/or high LCL heights. *Weather and Forecasting* **21**, 579-594.

Davies-Jones R.P., 1974: Discussion of measurements inside high-speed thunderstorm updrafts. *J. Appl. Meteor.*, **13**, 710-717.

Donaldson R.J., 1970: Vortex Signature Recognition by a Doppler Radar. *Journal of Applied Meteorology*, **9**, 661–670.

Dupilka M.L., G.W. Reuter, 2006a: Forecasting tornadic thunderstorm potential in Alberta using environmental sounding data. Part I: Wind shear and buoyancy. *Weather and Forecasting* **21**, 325-335.

Dupilka M.L., G.W. Reuter, 2006b: Forecasting tornadic thunderstorm potential in Alberta using environmental sounding data. Part II: Helicity, precipitable water, and storm convergence. *Weather and Forecasting* **21**, 336-346.

Eilts, M.D., l997: Overview of the Warning Decision Support System (WDSS). *Proc., 28th Conf. On Radar Meteor.*, Amer. Meteor. Soc., Boston, 404-405.

Freud E., Rosenfeld D., Meinrat O.Andreae ,Alexande A.Costa and Paulo Artaxo, 2005: Observed robust relations between CCN and vertical evolution of cloud drop size distributions in deep convective clouds. *Atmos. Chem. Phys. Discuss*., **5**, 10155-10195. http://www.copernicus.org/EGU/acp/acpd/5/10155/acpd-5-10155.htm

Friday, E. W. Jr., l994: The modernization and restructuring of the National Weather Service: An overview. *Bull. Am. Meteor. Soc.*, 75(1), 43-52.

Fridlind, A. M., A. S. Ackerman, E. J. Jensen, A. J. Heymsfield, M. R. Poellot, D. E. Stevens, D. Wang. L. M. Miloshevich, D. Baumgardner, R. P. Lawson, J. C. Wilson, R. C. Flragan, J. H. Seinfeld, H. H. Jonsson, T. M. VanReken, V. Varatbangkul, and T. A. Rissman, 2004: Evidence for the predominance of mid-tropospheric aerosols as subtropical anvil nuclei. *Science*. **304,** 718-722.

Golden, J.H., and C. R. Adams, 2000: The tornado problem: Forecast, Warning, and Response. *Natural Hazards Review*, Vol. 1(2), 107-118.

Hamill T.M., A.T. Church, 2000: Conditional probabilities of significant tornadoes from RUC-2 Forecasts. *Weather and Forecasting* **15**, 461-475.

Heymsfield, A. J, L. M. Miloshevich, C. Schmitt, A. Bansemer, C. Twohy, M. R. Poellot, A. Fridlind, and H. Gerber, 2005: Homogeneous ice nucleation in subtropical and tropical convection and

its Influence on cirrus anvil microphysics. *J. Atmos. Sci*., **62**, 41–64.

Heymsfield G.M., G. Szejwach, S. Schotz, R.H. Blackmer Jr., 1983: Upper-level structure of Oklahoma Tornadic storms on 2 May 1979. II: Proposed explanation of V pattern and internal warm region in infrared observations. *J. Atmos. Sci*., **22**, 1756-1767.

Houghton, J. T., L. G. Meira Filho, J. Bruce, Hoesung Lee, B. A. Callander, E. Haites, N. Harris, and K. Maskell, 1994: Climate Change 1994 – Radiative forcing of climate change and an evaluation of the IPCC IS92 Emission Scenarios. Reports of working groups I and II of the Intergovernmental Panel on Climate Change. Cambridge University Press, 339p.

Jensen, E. J., and A. S. Ackerman (2006), Homogeneous aerosol freezing in the tops of high-altitude tropical cumulonimbus clouds, Geophys. Res. Lett., 33, L08802, doi:10.1029/2005GL024928.

Johnson, J. T., Priegnitz, D., Witt, A., Wyatt, A., and Hondl, K., l997: The NSSL warning decision support system: Field testing and planning for AWIPS. *Proc., 28th Conf. On Radar Meteor.*, Amer. Meteor. Soc., Boston, 428-429.

Kaufman Y. J., and R. S. Fraser, 1997: The effect of smoke particles on clouds and climate forcing. *Scienc*e, **27**7(5332): 1636-1638.

Khain A. P., D. Rosenfeld and A. Pokrovsky, 2001: Simulating convective clouds with sustained supercooled liquid water down to -37.5^{o}C using a spectral microphysics model. Geophysical Research Letters, 28, 3887-3890.

Lensky I. M., D. Rosenfeld, 2006. The time-space exchangeability of satellite retrieved relations between cloud top temperature and particle effective radius. *Atmos. Chem. Phys.* **6,** 2887-2894.

Levizzani, V., M. Setvák, 1996: Multispectral, high-resolution satellite observations of plumes on top of convective storms. *J. Atmos. Sci.*, **53**, pp 361-369.

Lindsey D.T., D.W. Hillger, L. Grasso, J.A. Knaff, and J.F. Dostalek, 2006: GOES Climatology and Analysis of Thunderstorms with Enhanced 3.9-□ m Reflectivity. Monthly Weather Review, 134, 2342-2353.

Madalla, G.S., 1983: Limited Dependent and Qualitative Variables in Econometrics, ISBN-13: 9780521241434, Cambridge Univ. Press, 416p.

McCann, D.W., 1983: The enhanced-V, a satellite observable severe storm signature. *Mon. Wea. Rev*., **111**, 887-894.

Nakajima, T., and M. D. King, 1990: Determination of the optical thickness and effective particle radius of clouds from reflected solar radiation measurements. Part I: Theory. *J.Atmos. Sci.*, **47,** 1878-1893.

Pinsky, M. and Khain, A. P. 2002: Effects of in-cloud nucleation and turbulence on droplet spectrum formation in cumulus clouds. Q. J. R. Meteorol. Soc., 128, 1–33.

Pinsky M. B., A. P. Khain, D. Rosenfeld, and A. Pokrovsky, 1998: Comparison of collision velocity differences of drops and graupel particles in a very turbulent cloud. *Atmospheric Research*, **49**, 99-113.

Rasmussen E.N., D.O. Blanchard, 1998: A baseline climatology of sounding-derived supercell and tornado forecast parameters. *Weather and Forecasting*, **13**, 1148-1164.

Rosenfeld D. and G. Gutman, 1994: Retrieving microphysical properties near the tops of potential rain clouds by multispectral analysis of AVHRR data. *Atmospheric Research*, **34**, 259-283.

Rosenfeld D. and I. M. Lensky, 1998: Satellite-based insights into precipitation formation processes in continental and maritime convective clouds. The *Bulletin of American Meteorological Society*, **79**, 2457-2476.

Rosenfeld D. and W. L. Woodley, 2000: Deep Convective Clouds with Sustained Supercooled Liquid Water Down to –37.5°C. *Nature*, **405**, 440-442.

Rosenfeld D., R. Lahav, A. P. Khain, M. Pinsky, 2002: The role of sea-spray in cleansing air pollution over ocean via cloud processes. *Science*, **297**, 1667-1670.

Rosenfeld D. and W. L. Woodley, 2003: Closing the 50-year circle: From cloud seeding to space and back to climate change through precipitation physics. Chapter 6 of "Cloud Systems, Hurricanes, and the Tropical Rainfall Measuring Mission (TRMM)" edited by Drs. Wei-Kuo Tao and Robert Adler, 234pp., p. 59-80, *Meteorological Monographs* **51**, AMS.

Rosenfeld D., 2006: Aerosol-Cloud Interactions Control of Earth Radiation and Latent Heat Release. *Space Science Reviews*. Springer, 9p. 6 December 2006. DOI: 10.1007/s11214-006-9053-6. http://dx.doi.org/10.1007/s11214-006-9053-6

Rosenfeld D., M. Fromm, J. Trentmann, G. Luderer, M. O. Andreae4, and R. Servranckx, 2006a: The Chisholm firestorm: observed microstructure, precipitation and lightning activity of a pyro-Cb. *Atmos. Chem. Phys. Discuss*., **6**, 9877–9906, 2006.

Rosenfeld D., W. L. Woodley, T. W. Krauss, V. Makitov, 2006b: Aircraft Microphysical Documentation from Cloud Base to Anvils of Hailstorm Feeder Clouds in Argentina. *J. Appl. Meteor*., **45**, 1261–1281, September 2006.

Rosenfeld, D., W. L. Woodley, A. Lerner, G. Kelman, and D. T. Lindsey (2008), Satellite detection of severe convective storms by their retrieved vertical profiles of cloud particle effective radius and thermodynamic phase, *J. Geophys. Res.*, **113**, D04208, doi:10.1029/2007JD008600

Setvák M., Rabin R.M., Doswell C.A., Levizzani V., 2003: Satellite observations of convective storm top features in the 1.6 and 3.7/3.9 μm spectral bands. Atmos. Research, 67-68C, 589-605.

Smith, S.B., Goel, S.K., Fillaggi, M.T., Churma, M.E., and Xin, L., 1999: Overview and status of the AWIPS system for convection analysis and nowcasting (SCAN). *Proc.,15th Int. Conf. On Interactive Information and Processing Sys. For Meteorology, Oceanography, and Hydro.,* Amer. Meteor. Soc., Boston, 326-329.

Stith, J. L., J. A. Hagerty, A. J. Heymsfield, and C. A. Grainger, 2004: Microphysical characteristics of tropical updrafts in clean conditions. *J. Appl. Meteor*., **43**, 779-794.

Weisman, M. L., and J. B. Klemp, 1984: The structure and classification of numerically simulated convective storms in directionally varying wind shears. Mon. Wea. Rev., 112, 2479–2498.

Wilson, A., Rodgers, D.M., and Grote, U.H., 1999: Adding productivity tools to the WFO-Advanced meteorological workstation. *Proc., 15th Int. Conf. On Interactive Information and Processing Sys. for Meteorology, Oceanography, and Hydro.,* Amer. Meteor. Soc., Boston, 322-325.

Woodley, W.L., D. Rosenfeld, G. Kelman and J.H. Golden, 2008: Short-Term Forecasting of Severe Convective Storms Using Quantitative Multi-Spectral, Satellite Imagery. Final Report to the NOAA SBIR Program office for SBIR Phase 2, 127 pp.